Author Manuscript

Author Manuscript

Author Manuscript

Author Manuscript

HHS Public Access

Author manuscript

Nature. Author manuscript; available in PMC 2024 May 01.

Published in final edited form as:

Nature. 2023 November ; 623(7985): 122–131. doi:10.1038/s41586-023-06627-y.

Cholinergic neurons trigger epithelial Ca^{2+} currents to heal the gut

Afroditi Petsakou[1,*], **Yifang Liu**[1], **Ying Liu**[1], **Aram Comjean**[1], **Yanhui Hu**[1], **Norbert Perrimon**[1,2,*]

[1]Department of Genetics, Harvard Medical School, Boston, USA

[2]Howard Hughes Medical Institute, Boston, USA

Abstract

A fundamental and unresolved question in regenerative biology is how tissues return to homeostasis after injury. Answering this question is essential for understanding the etiology of chronic disorders such as inflammatory bowel diseases and cancer[1]. We used the *Drosophila* midgut[2] to investigate this and discovered that during regeneration a subpopulation of cholinergic[3] neurons triggers Ca^{2+} currents among intestinal epithelial cells, the enterocytes, to promote return to homeostasis. We found that down-regulation of the conserved cholinergic enzyme Acetylcholinesterase[4] in the gut epithelium enables acetylcholine from specific TNF/Egr[5]-sensing cholinergic neurons to activate nicotinic receptors in innervated enterocytes. This activation triggers high Ca^{2+} that spreads in the epithelium through Inx2/Inx7 gap junctions[6], promoting enterocyte maturation followed by reduction of proliferation and inflammation. Disrupting this process causes chronic injury consisting of ion imbalance, Yki/Yap activation[7], cell death and increase of inflammatory cytokines reminiscent of inflammatory bowel diseases[8]. Altogether, the conserved cholinergic pathway facilitates epithelial currents that heal the intestinal epithelium. Our findings demonstrate nerve- and bioelectric[9]-dependent intestinal regeneration and advance our current understanding of how a tissue returns to homeostasis after injury.

The cholinergic pathway is an ancient conserved pathway used by peripheral neurons to communicate with internal organs[3]. The two cholinergic receptors, nicotinic and muscarinic, and enzymes modulating acetylcholine (ACh) metabolism, e.g. Acetylcholinesterase (AChE/Ace), are highly conserved and expressed in non-neuronal tissues[3]. Cholinergic receptors regulate ion transport in the intestinal epithelium which is vital for water and nutrient absorption[10]. Recently, attention has been given to the anti-inflammatory properties of the cholinergic pathway, with reduced ACh responsiveness associated with intestinal diseases[11].

Reprints and permissions information is available at www.nature.com/reprints.

[*]Correspondence and requests for materials should be addressed to Afroditi Petsakou: Afroditi_Petsakou@hms.harvard.edu; Norbert Perrimon: perrimon@genetics.med.harvard.edu.

Author Contributions: Conceptualization: AP, NP; Methods, Data Acquisition, Resources, Visualization and Imaging: AP; Independent replication of experiments at Harvard Medical School: AP; FACs sorting: YL, AP; Analysis of single nuclei data: YL, YH, AC, AP ; Writing – original draft: AP, Writing – review, editing & revising: AP, NP.

All authors declare that they have no competing interests.

Supplementary Information and Source Data Files are available for this paper.

Author Manuscript Author Manuscript Author Manuscript Author Manuscript

The *Drosophila* midgut, equivalent to mammalian small intestine, has been used to identify conserved molecular pathways that trigger inflammation and regeneration in the injured epithelium[1,12]. The midgut epithelium is single-layered and comprised of enterocytes (ECs), large polyploid epithelial cells specialized in absorption, secretory enteroendocrine cells (EEs) and progenitor cells (PCs)[2,13,14]. The visceral muscle and trachea surround the midgut epithelium, whereas anterior and posterior midgut regions are innervated by enteric neurons[2]. When the epithelium is injured, intestinal stem cells (ISCs) divide rapidly, giving rise to daughter cells (EBs) that differentiate into ECs and EEs[2]. Depending on the injury or infection, a multifaceted interplay of conserved inflammatory and regenerative pathways (e.g., EGFR, JAK-STAT, Wnt, BMP, Yki/Yap) activate ISC proliferation so that a sufficient PC (ISC/EB) pool replenishes the epithelium[15]. Despite the in-depth understanding of how repair is triggered, it is unclear how these pathways are dampened once the epithelium transitions to homeostasis. Following specific damage, the BMP pathway has been reported to have dual roles first promoting proliferation and later ISC-quiescence[16,17].

Here, we provide evidence for the fundamental role of an epithelial bioelectric mechanism controlled by cholinergic neurons that occurs as the midgut transitions from colitis-like injury to homeostasis – a phase we refer to as recovery. We show that during recovery, ECs become more sensitive to ACh by downregulating *Ace* and upregulating *nAChR subunit β3* (*nAChRβ3*). Also, specific TNF/Egr-regulated cholinergic neurons, that we refer to as ARCENs, strengthen the axonal properties of their enteric innervations. We demonstrate that transition to homeostasis relies on the healing functions of nAChR-mediated Ca^{2+} currents among ECs, that spread through Inx2/Inx7 gap junctions and are triggered by local ARCEN-EC cholinergic signaling.

ECs are sensitive to ACh during recovery

To study the *Drosophila* intestinal epithelium while it transitions to homeostasis after injury, we damaged the gut with dextran sodium sulfate (DSS), then returned flies to standard food. DSS induces colitis in mammals[8] and has been used in *Drosophila* to identify conserved proliferative pathways[15]. We fed flies DSS for 4 days (injury) followed by two or four days of standard food (recovery, Fig.1a). Gut damage elevated the expression of effector *Drosophila* caspase 1 (Dcp1), indicative of cell death (Fig.1b), and of conserved inflammatory cytokines such as IL6-like *unpaired 3* (*upd3*)[18] and TNF homolog *eiger (egr)*[5] (Ext. Data Fig.1a), resembling DSS-induced colitis[8]. Once flies were transferred to standard food, the epithelium required 4 days to return to homeostasis as determined by the levels of i) inflammatory cytokines (Ext. Data Fig.1a), ii) cell death (Fig.1b), iii) ISC proliferation (with mitotic marker anti-phospho-Histone3 (pH3), Fig. 1c), and iv) expression of PC marker *escargot* (*esg*; Ext. Data Fig.1b) and two markers of mature cells, *pdm1*, marker of ECs, and *prospero* (*pros*), marker of EEs (Ext. Data Fig.1b).

To search for recovery-specific differentially expressed genes, we performed snRNAseq on the 2nd day of recovery (Ext. Data Fig.1c). We identified 14 clusters from 8073 nuclei recovered, which we assigned to different epithelial and progenitor cell populations, as well as to cardia and LFC/Cu/Fe gut cells (Ext. Data Fig.1c-e). We analyzed differential gene expression between homeostasis and recovery and observed that *Ace*, is highly enriched in

Author Manuscript Author Manuscript Author Manuscript Author Manuscript

ECs and significantly downregulated during recovery (Ext. Data Fig.1f, Ext. Data Fig.2a-b, S. Table 1-2). Ace hydrolyzes ACh to choline and acetate and thus defines a cell's sensitivity to ACh.

We observed ~75% reduction of *Ace* during recovery (Fig.1d). Previous intestinal RNA-seq profiling after bacterial infections also detected *Ace* downregulation (Flygut-EPFL data)[19], which we confirmed (Ext. Data Fig.2c). Next, we challenged the gut with injury-inducing chemical Bleomycin which triggers different pathways as compared with DSS[20]. This led to significant *Ace* decrease (Ext. Data Fig.2c), indicating that *Ace* downregulation occurs consistently after different types of intestinal epithelial damage.

To test the role of *Ace* during regeneration, we used CRISPR/Cas9 activation (Ext. Data Fig.2d). We found that 4 days of *Ace* overactivation in ECs (using the Gal4 *myo1A*-driver together with the repressor *Tubulin*-Gal80^{TS}, referred as *myo1A^{TS}*) led to excessive ISC proliferation during recovery (Fig.1e), while same activation during homeostasis or injury did not affect proliferation (Fig.1e). Similarly, consecutive DSS challenges while *Ace* is conditionally overexpressed in ECs using the *myo1A^{TS}* or *mex^{TS}* driver (another EC driver) led to recovery-specific ISC over-proliferation (Fig.1f, Ext. Data Fig.2e). We next tested if *Ace* perturbations in visceral muscle or immune cells regulate ISC proliferation, which they did not (Ext. Data Fig.2f). These findings reveal that overexpressing *Ace* in ECs during recovery prevents ISCs from becoming quiescent, causing an excessive regenerative response. We next tested whether the role of *Ace* during recovery is consistent after different types of epithelial damage. Overexpressing *Ace* in ECs after *Ecc15* infection or Bleomycin-injury consistently caused over-proliferation (Ext. Data Fig.2g-h).

ACh has been proposed to modulate ion transport in the intestinal epithelium in a Ca^{2+}-dependent manner[10]. Thus, to test for epithelial changes in ACh sensitivity during homeostasis and recovery, we visualized Ca^{2+} by conditionally expressing the Ca^{2+} indicator GCAMP*7c*[21] in ECs. Using *ex vivo* live imaging, we found that Ca^{2+} levels in ECs are significantly higher during recovery following ACh administration than during homeostasis and that this is attenuated upon overexpression of *Ace* (Fig.1g, Ext. Data Fig.2i and Videos S1-S3). These results indicate that during recovery ECs become more sensitive to ACh by decreasing *Ace* and this change is required for transition to homeostasis after injury.

nAChRβ3 is required in ECs for recovery

Cholinergic receptors are G-protein-coupled muscarinic receptors (mAchR) or ligand-gated ion channel nicotinic receptors (nAChR) made of five homomeric or heteromeric subunits (α1, α2, α3, α4, α5, α6, α7, β1, β2 or β3). To identify which cholinergic receptor becomes activated during recovery, we screened all nAChR subunits and different mAchR subtypes by knocking down their expression in ECs. Conditional RNAi expression targeting *nAChRβ3* in ECs caused over-proliferation during recovery (Fig.2a-b, Ext. Data Fig.3a-c) and after *Ecc15* infection (Ext. Data Fig.3d). Furthermore, *nAChRβ3* knockdown in ECs combined with repeated DSS-injury (Recovery 2x) led to hyperplasia (Fig.2b-c). Conditional knockdown of *nAChRβ3* in ECs significantly reduced the Ca^{2+} response after ACh administration during recovery (Ext. Data Fig.3e, Ext. Data Fig.3j). Together,

Author Manuscript Author Manuscript Author Manuscript Author Manuscript

these data suggest that reducing *nAChRβ3* in ECs leads to phenotypes resembling *Ace* upregulation. This effect is specific to ECs, as conditionally knocking down *nAChRβ3* in PCs, EBs alone, EEs, visceral muscle or hemocytes had no effect on proliferation (Ext. Data Fig.3f).

The profiling depth of our snRNAseq was not sufficient to conclude if *nAChRβ3* expression is altered between homeostasis and recovery, despite being solely found in ECs (Ext. Data Fig.3g). To visualize the expression of nAChRβ3, we inserted a Flag tag within nAChRβ3 (nAChRβ3-flag) (Fig.2d, Ext. Data Fig.3h). Endogenous nAChRβ3 was significantly enriched in ECs by day 2 of recovery (Fig.2d), whereas a decrease in *nAChRβ3* levels coincided with return to homeostasis (Ext. Data Fig.3i). nAChRβ3 was localized to the basal side of ECs and some ECs had more nAChRβ3 clustered on their basal side (Fig.2d-e).

Next, we administered the cholinergic agonist nicotine, which activates nAChRs and cannot be hydrolyzed by Ace. Nicotine administration significantly increased Ca^{2+} in ECs during recovery compared to homeostasis, reminiscent of ACh-sensitivity, and this was diminished when *nAChRβ3* was knocked down (Fig.2f-g, Ext. Data Fig.3k and Videos S4-S6). We conclude that *nAChRβ3* in ECs is essential for gut recovery and recovery-specific enrichment of nAChRβ3 provides an additional level of regulation that likely renders ECs more responsive to ACh while the epithelium transitions to homeostasis.

nAChRβ3-mediated Ca^{2+} promotes recovery

ISC proliferation can be triggered by the release of cytokines which vary depending on the stimulus[15]. To identify pathways responsible for unrestrained proliferation during recovery after *nAChRβ3* knockdown in ECs, we tested the expression of known cytokines (Fig.3a, Ext. Data Fig.4a-b). We detected *unpaired 2* (*upd2*) and *upd3* JAK-STAT ligands, together with EGF-like ligand *vein* (*vn*) and *egr*, to be significantly upregulated (Fig.3a, Ext. Data Fig.4a-b). Egr is associated with cell death[22], whereas Upd2, Upd3 and Vn are up-regulated on activation of the Hippo pathway effector Yorkie (Yki/YAP) in damaged ECs[23,24]. Supporting this, knocking down *nAChRβ3* in ECs during recovery significantly increased cell death (Ext. Data Fig.4c) as well as expression of Yki targets *Diap1* and *Ex* (Ext. Data Fig.4d-e). Also, knockdown of *nAChRβ3* during recovery significantly reduced the transcript and protein levels of *pdm1* (Fig. 3b, Ext. Data Fig.4f-g), while *pros* remained unchanged (Ext. Data Fig.4h). These data suggest that disruption of nAChRs in ECs during recovery impairs ECs, leading to cell death, Yki activation and subsequent production of inflammatory signals that induce unwarranted ISC proliferation.

Cholinergic receptors regulate ion transport in the mammalian epithelium[10,25]. We asked whether nAChRs have similar functions in ECs using dyes that detect Na^+ (SodiumGreen) or Cl^- (MQAE), and the Ca^{2+} transcriptional reporter NFAT-CalexA[26]. Reduction of *nAChRβ3* during recovery caused significant ion imbalance in the epithelium, with reduced Cl^- and Na^+ levels (Ext. Data Fig.4i). We observed that Ca^{2+} is significantly upregulated the first day of recovery before returning to levels resembling homeostasis (Fig.3c). This endogenous Ca^{2+} increase disappears when *nAChRβ3* is knocked down in ECs (Fig.3d). Also, Ca^{2+} increase occurs only in ECs during recovery, as ISCs that use Ca^{2+} for

Author Manuscript Author Manuscript Author Manuscript Author Manuscript

proliferation[27,28] show Ca^{2+} decline during recovery (Ext. Data Fig.4j). To examine the importance of nAChR-mediated Ca^{2+} during recovery, we genetically compensated for Ca^{2+} in *nAChRβ3*-deficient ECs. Conditional overexpression of Ca^{2+} channel Orai combined with knockdown of *nAChRβ3* in ECs was sufficient to restore i) ISC proliferation (Fig.3e, Ext. Data Fig.5a), ii) the number of pdm1+ ECs (Fig.3f, Ext. Data Fig.5b), and iii) Cl^- (Ext. Data Fig.5c) to levels identical to controls. Next, we over-expressed the vertebrate Ca^{2+} buffer protein parvalbumin (PV) in ECs to reduce the amount of intracellular Ca^{2+} for four days during recovery (Ext. Data Fig.5d). This led to over-proliferation during recovery while having no effect during homeostasis (Ext. Data Fig.5d), supporting the importance of Ca^{2+} in ECs during recovery.

To further study the effect of *nAChRβ3* during gut regeneration, we generated flies that overexpress *nAChRβ3* in ECs using the Gal4 or LexA system (*UAS- nAChRβ3* and *LexAop-nAChRβ3*, Ext. Data Fig.5e-f). Also, we generated an EC-LexA driver (*mex-LexA::GAD*) together with *Tubulin*-$Gal80^{TS}$, referred as $mexLexA^{TS}$ (Ext. Data Fig.5f). Conditionally overexpressing *nAChRβ3* in ECs during homeostasis doubles the amount of Ca^{2+} in ECs after nicotine administration (Ext. Data Fig.5g). Also, *nAChRβ3* overexpression in ECs significantly expedited recovery, with ISC proliferation and *pdm1* expression reaching levels indistinguishable from unchallenged guts at two days, half the expected time (Fig.3g-h). *nAChRβ3* overexpression in ECs during homeostasis and injury did not change ISC proliferation (Fig.3g). Additionally, overexpressing *nAChRβ3* in ECs during recovery significantly reduced inflammatory cytokine levels and cell death (Fig.3i, Ext. Data Fig.5h-j).

Together, our data show that high intracellular Ca^{2+} in ECs triggered by nAChRs control intestinal epithelium recovery by promoting EC maturation and ion balance. Disruption of nAChR-mediated Ca^{2+} causes EC deficiency, ion imbalance, elevated cell death and Yki activation, followed by over-inflammation and over-proliferation. In contrast, increasing Ca^{2+} in ECs via overexpressing *nAChRβ3* expedites return to homeostasis by advancing EC maturation and decreasing cell death, subsequently reducing inflammation and proliferation.

Neuro-EC interactions promote recovery

ACh is released by neuronal and non-neuronal cells that express *ChAT* (*Choline acetyltransferase*), the enzyme that catalyzes ACh synthesis[3]. To identify the source of ACh responsible for nAChR-mediated recovery, we first tested midgut cells (PCs, ECs, EEs), the visceral muscle and immune cells (hemocytes). ISC proliferation during recovery remained unaffected when *ChAT* was conditionally knocked down in these cells (Ext. Data Fig.6a). Similarly, EE-less guts[29] do not over-proliferate during recovery (Ext. Data Fig.6b). Altogether, these data point to a neuronal source of ACh. The importance of neurons during regeneration has been reported in different tissues[30]. For the gut, studies have highlighted the anti-inflammatory properties of mammalian enteric neurons[31,32], while limited associations have been made between neurons and ISC proliferation in *Drosophila*[33,34].

Author Manuscript Author Manuscript Author Manuscript Author Manuscript

Since ACh is a short-distance neurotransmitter/local neurohormone, the most likely source during recovery is the enteric nervous system. *Drosophila* enteric neurons innervate the midgut in anterior (R1, R2) and posterior regions (R4, R5), even though their cell bodies reside in the brain, hypocerebral ganglion (HCG), or the adult ventral nerve cord (VNC)[2]. Also, enteric innervations reach the intestinal epithelium[34]. To identify a driver for cholinergic enteric neurons, we screened a set of neuronal drivers (FlyLight)[35]. We identified a Gal4 driver, *R49E06-Gal4*, that is expressed in ~43 neurons in the abdominal ganglion of the VNC (Ext. Data Fig.6c-g), has no expression in the gut, and very limited expression in the brain (Ext. Data Fig.6c&FlyLight). We tested the cholinergic nature of *R49E06*-neurons using the cholinergic Gal80 repressor (ChAT-Gal80), which inhibited GFP expression in most VNC *R49E06*-neurons (Ext. Data Fig.6d). We found that ~35 of the ~43 neurons in the abdominal ganglia are ChAT+/cholinergic (Ext. Data Fig.6e-f) and in their majority do not express Prospero (Pros, Ext. Data Fig.6g). We observed that some R49E06-neurons innervate the midgut and are ChAT+ (Ext. Data Fig.6h), suggesting that a subpopulation of *R49E06*-neurons are cholinergic enteric neurons. To confirm that *R49E06*-innervations can release ACh to the gut, we used an antibody against the synaptic vesicle membrane protein Synaptotagmin1 (Syt1) which is essential for neurotransmitter release. We observed that R49E06-innervations run between the muscle and intestinal epithelium while carrying Syt1+ swellings (Ext. Data Fig.6i). We refer to Syt1+ swellings as presynaptic boutons because they resemble *en passant* varicosities described in the autonomous nervous system and are located at sites where a neurotransmitter diffuses to receptors located in nearby (innervated) cells. Together these data indicate that *R49E06*-neurons are in their majority cholinergic and include a subpopulation of cholinergic enteric neurons that innervate the intestinal epithelium and muscle.

To further characterize *R49E06*-enteric innervations, we sectioned flies with a vibratome so that innervations and gut remained intact (Fig.4a). R49E06-neurons innervate the midgut at distinct locations in R2, R4 and R5 (Fig.4a). To distinguish between the axonal and dendritic domains, we expressed the synaptic vesicle marker Syt1HA and the dendritic indicator DenMark for two days during recovery. We observed that Syt1HA accumulated at the terminal of *R49E06*-innervations in the vicinity of the gut (Fig.4a, Ext. Data Fig.6j), whereas DenMark accumulated upstream (Ext. Data Fig.6k). We observed that Syt1HA-innervations are close to ECs (Fig.4b, Ext. Data Fig.6l and Video S7), suggesting that *R49E06* neurons innervate ECs and could be the source of ACh.

To test whether R49E06 neurons regulate gut regeneration, we conditionally knocked down *ChAT* in these neurons. This caused: i) over-proliferation during recovery and after repetitive DSS-injury (Fig.4c), (ii) recovery-specific reduction of *pdm1* (Fig. 4d), iii) no significant change of *pros* (Ext. Data Fig.7a), and iv) elevated expression of inflammatory cytokines during recovery (Ext. Data Fig.7b). Also, co-expression of the VNC repressor *Tsh*-Gal80[36], while reducing *ChAT* in R49E06-neurons, prevented ISC over-proliferation during recovery (Ext. Data Fig.7c). Further, *ChAT* decrease in R49E06 neurons led to ISC over-proliferation after *Ecc15* infection (Ext. Data Fig.7d). Thus, reduction of ACh synthesis from R49E06-neurons in VNC leads to lasting unresolved injury, resembling *nAChRβ3*-deficiency in ECs. These data indicate that intestinal repair is under neuronal control, leading us to name these neurons Anti-inflammatory Recovery-regulating Cholinergic Enteric Neurons (ARCENs).

Author Manuscript Author Manuscript Author Manuscript Author Manuscript

To test whether ARCENs are required for nAChR-mediated recovery, we blocked neurotransmitter release with the *UAS-shibire^{TS}* transgene while simultaneously overexpressing *nAChRβ3* (Fig.4e). We found that 24hr expression of *shibire^{TS}* in ARCENs was sufficient to prevent *nAChRβ3* overexpression in ECs from rapidly decreasing proliferation (Fig.4e). To verify that ARCENs release ACh to the intestinal epithelium, we overexpressed the ion channel *TrpA1* and thermo-genetically depolarized ARCENs (Ext. Data Fig.7e). TrpA1-mediated induction of ARCENs the first 6 hours of recovery significantly reduced ISC proliferation, whereas additionally expressing the cholinergic repressor *ChAT*-Gal80 restored proliferation to levels identical to controls (Ext. Data Fig.7e). Also, TrpA1-induction of ARCENs significantly reduced the expression of gut inflammatory cytokines (Ext. Data Fig.7f). Moreover, we used the QF system to generate R49E06-QF (ARCEN-QF) driver (Ext. Data Fig.7g). We used ARCEN-QF together with light-gated cation channel CsChrimson to depolarize ARCENs while conditionally expressing in ECs the Ca^{2+} transcriptional reporter *NFAT-CaLexA* (Fig.4f). Optogenetic activation of ARCENs the first 6 hours of recovery was sufficient to significantly increase endogenous Ca^{2+} and levels of pdm1+ ECs (Fig.4f). Together, these data support that ARCENs provide ACh to ECs to promote transition to homeostasis after injury by activating nAChR-mediated Ca^{2+} influx, increasing mature ECs, reducing proliferation, and decreasing inflammation in the intestinal epithelium. However, we cannot completely rule out that the subpopulation of ARCENs without enteric innervations may have mediator roles that promote recovery by activating non-ARCEN cholinergic enteric innervations. Our findings demonstrate nerve-dependent intestinal regeneration, placing the intestinal epithelium among the tissues whose ability to regenerate depends on neurons.

ARCENs depend on TNF signaling

The cholinergic anti-inflammatory reflex has been proposed to sense inflammatory signals like TNF and reduce them by triggering ACh release across neuro-immune interactions[11,37]. As *Drosophila* peripheral neurons have been reported to respond to Egr through *wengen* (*wgn*)[38], one of the two known Egr receptors (*wgn* and *grindelwald, grnd*)[39,40], we tested whether the protective role of ARCENs is linked to Egr. Reduction of *wgn* but not *grnd* in ARCENs led to significant ISC over-proliferation specifically during recovery, which was rescued when *Tsh-Gal80* was co-expressed (Fig.4g, Ext. Data Fig.7h).

We searched for the source of TNF signaling by conditionally knocking down *egr* in gut and immune cells (Ext. Data Fig.7i). Reduction of *egr* in PCs and ECs did not impact ISC proliferation during recovery and knocking down *egr* in hemocytes caused under-proliferation (Ext. Data 7i). However, decreasing *egr* in all three populations concurrently caused significant over-proliferation during recovery (Ext. Data Fig.7i-j). This suggests that ARCENs likely sense Egr from multiple sources. Also, knocking down *egr* in all three cell populations during injury caused ISC under-proliferation (Ext. Data Fig.7j), consistent with the proposed proliferative role of Egr[41].

Further, we tested whether secreted Egr reaches ARCENs. We expressed in the transmembrane of ARCENs an extracellular nanobody-based GFP trap (morphotrap)[42] for two days during recovery while endogenous Egr was fused to GFP (Egr-GFP). We observed

Author Manuscript Author Manuscript Author Manuscript Author Manuscript

GFP accumulation in ARCEN-projections expressing the morphotrap (Ext. Data Fig.7k), indicating that secreted Egr reaches ARCENs. GFP accumulation was only observed in ARCEN-projections near the posterior midgut and not near the VNC (Ext. Data Fig.7k). Since near the posterior midgut ARCEN-innervations are enriched with dendritic sites (Ext. Data Fig.6k), this raises the possibility that wgn receptors are present in this region and ARCENs likely sense Egr through their enteric projections during recovery. As TNF has been proposed to promote synaptic plasticity and strengthening[43] and axonal strengthening is associated with elevated firing[44], we examined whether existing synaptic boutons of ARCEN-innervations undergo Egr-dependent changes (Fig.4h). ARCEN-innervations undergo significant increase in density and volume of synaptic boutons during recovery compared to homeostasis (Fig. 4h). This increase is diminished upon *wgn* reduction (Fig.4h), indicating that ARCEN-innervations respond to Egr by strengthening their axonal properties, likely to boost ACh release. Altogether, our data support that the function of ARCENs during gut regeneration is linked to TNF signaling, reminiscent of the cholinergic anti-inflammatory reflex[37].

Ca^{2+} spreads via Inx2/Inx7 gap junctions

We observed that opto-activation of ARCENs led to broad Ca^{2+} increase across ECs in the posterior gut (Fig.4f), despite the limited innervations, suggesting that Ca^{2+} likely propagates between innervated and non-innervated ECs. To test this, we performed *ex vivo* Ca^{2+} live imaging utilizing split-Gal4 drivers[45] that when combined are specific to a small population of ECs between R4 and R5 (R4c, Ext. Data Fig.8a), which we refer as spECs. We transiently increased Ca^{2+} in spECs using the light-gated CsChrimson channel, while recording Ca^{2+} changes in neighboring ECs (Fig. 5a, Ext. Data Fig.8b). Activation of CsChrimson in spECs increased Ca^{2+} in distant ECs as far as 180μm (Fig.5a, Ext. Data Fig.8b, Video S8) and the gap junction blocker Heptanol, significantly reduced Ca^{2+} propagation (Ext. Data Fig.8b). These data suggest that when Ca^{2+} is elevated in a subpopulation of ECs, gap junctions spread Ca^{2+} in more ECs. The endogenous flow of ions among cells (bioelectric signaling) has been proposed to regulate regeneration[9,46,47]. Therefore, we tested if generating Ca^{2+} currents via CsChrimson-activation in spECs could impact gut regeneration (Fig.5b). We found that 7hr opto-activation of spECs led to significantly faster decrease in proliferation the first day of recovery (Fig.5b), reminiscent of ARCEN activation (Ext. Data Fig.7e).

To investigate further how bioelectric signaling regulates gut recovery we analyzed in our single nuclei data the expression of innexins, the components of gap junctions in invertebrates[6,48]. *Innexin2* (*Inx2*) and *Innexin7* (*Inx7*) are similarly enriched in ECs whereas their expression in PC and EE clusters is lower (Ext. Data Fig.8c-e). We confirmed expression in ECs using an antibody for Inx2 (Ext. Data Fig.8f). *Inx7* reduction in ECs disrupted Inx2 gap junction formation (Ext. Data 8g-h), suggesting that Inx2 and Inx7 form heteromeric gap junctions. Moreover, knocking down *Inx2* or *Inx7* in ECs led to recovery-specific over-proliferation (Fig.5c-d), whereas no significant changes occurred during homeostasis or injury. Further, knocking down *Inx2* while opto-activating spECs prevented rapid decrease in ISC proliferation during recovery (Ext. Data Fig.8i). Also,

Author Manuscript Author Manuscript Author Manuscript Author Manuscript

knocking down *Inx2* or *Inx7* in ECs during recovery caused significantly reduced and irregular Ca^{2+} distribution together with significantly decreased $pdm1^{+}$ levels (Fig.5e).

Gap junctions are activated by membrane potential changes, including increases in intracellular Ca^{2+}[6]. This suggests that nAChR-induced Ca^{2+} during recovery could prompt gap junction activation in ECs. To test this, we overexpressed *nAChRβ3* for two days while knocking down *Inx2* in ECs during recovery (Fig.5f, Ext. Data Fig.8j). Knocking down *Inx2* was sufficient to attenuate rapid decrease in ISC proliferation and block fast increase of pdm1+ ECs, thereby blocking the expedited recovery triggered by *nAChRβ3* overexpression (Fig.5f, Ext. Data Fig.8j). Finally, we tested whether Inx2/Inx7 gap junctions facilitate Ca^{2+} responses in ECs during the nicotinic sensitivity assay. Conditionally reducing *Inx2* expression resulted in significantly dampened nicotine-triggered Ca^{2+} increase during recovery (Fig.5g, Ext. Data Fig.8k and Videos S9-S10). We observed that Ca^{2+} distribution among ECs was not only reduced but also uneven (Fig.5g, Ext. Data Fig.8k and Videos S9-S10). This suggests that during recovery gap junctions facilitate nAChR-induced Ca^{2+} to spread evenly among ECs. Altogether, our data support that Inx2/Inx7 gap junctions are required for nAChR-mediated Ca^{2+} to spread in ECs during recovery and that disruption of this bioelectric signaling prevents transition to homeostasis.

Discussion

We address a fundamental question, how does transition to homeostasis occur after injury? We found that the cholinergic pathway directs the gut to return to homeostasis by coordinating neuro-epithelial interactions and bioelectric signaling (Ext. Data Fig.9). Our findings reveal that nAChR-mediated high Ca^{2+} in ECs is essential for recovery (Fig.3, Ext. Data Fig.5). It is reported that Ca^{2+} increase after nAChR activation is augmented autonomously by opening of voltage gated Ca^{2+} channels and release of Ca^{2+} from intracellular stores[49]. This could occur in nAChR-activated ECs during recovery likely to assist in sufficiently elevating Ca^{2+}. We discovered that elevated Ca^{2+} from few ECs spreads via gap junctions to more ECs (Fig.5, Ext. Data Fig.8), which is consistent with a recent report of Ca^{2+} waves in R3 of the midgut[50]. The use of endogenous ion currents that electrically couple multiple cells so that they behave as one unit, has been linked to growth and tissue-patterning during development and regeneration[9,47]. Our study supports that bioelectric mechanisms regulate midgut regeneration to ensure that important physiological functions like ion transport are evenly restored across the epithelium.

Despite the increasing knowledge of protective anti-inflammatory roles for peripheral neurons, many aspects remain unclear[11]. We discovered that cholinergic signaling from ARCENs is required for the transition of the intestinal epithelium from injury to homeostasis (Fig.4, Ext. Data Fig.7). During recovery ARCEN-innervations undergo Egr-dependent synaptic strengthening (Fig.4h) and ECs change the levels of cholinergic components (Fig.1d, 2d-e). This coordinated plasticity, in neuro-epithelial cholinergic interactions likely occurs to control the initiation, strength, and duration of nAChR-mediated Ca^{2+} currents across the epithelium and precisely promote recovery. In addition, the cholinergic anti-inflammatory reflex has been proposed to be a cholinergic neuro-immune response that senses and counteracts inflammatory signals[11,37]. We propose that a similar mechanism

Author Manuscript Author Manuscript Author Manuscript Author Manuscript

exists in *Drosophila* and is regulated by ARCENs which reside in the posterior VNC, potentially the fly equivalent of vagus nerve. ARCENs sense Egr likely through their projections (Ext. Data Fig.6k, Ext. Data Fig.7k) and counteract gut inflammation and proliferation via neuro-EC cholinergic signaling (Fig.4, Ext. Data Fig.7). Altogether, our study broadens our current understanding of how regeneration ends by revealing how cooperation between peripheral neurons and epithelial bioelectric signaling directs a tissue towards homeostasis. This work may help identify the etiology of chronic intestinal diseases and provides a link between neurological disorders and intestinal pathologies.

Methods

Flies were crossed and raised between 19-23°C in standard fly food. All adult flies were tested 3-5 days after hatching. All experiments were done in female flies. Detailed description of experimental methods is found on Supplementary Information (SI).

Author Manuscript Author Manuscript Author Manuscript Author Manuscript

Extended Data

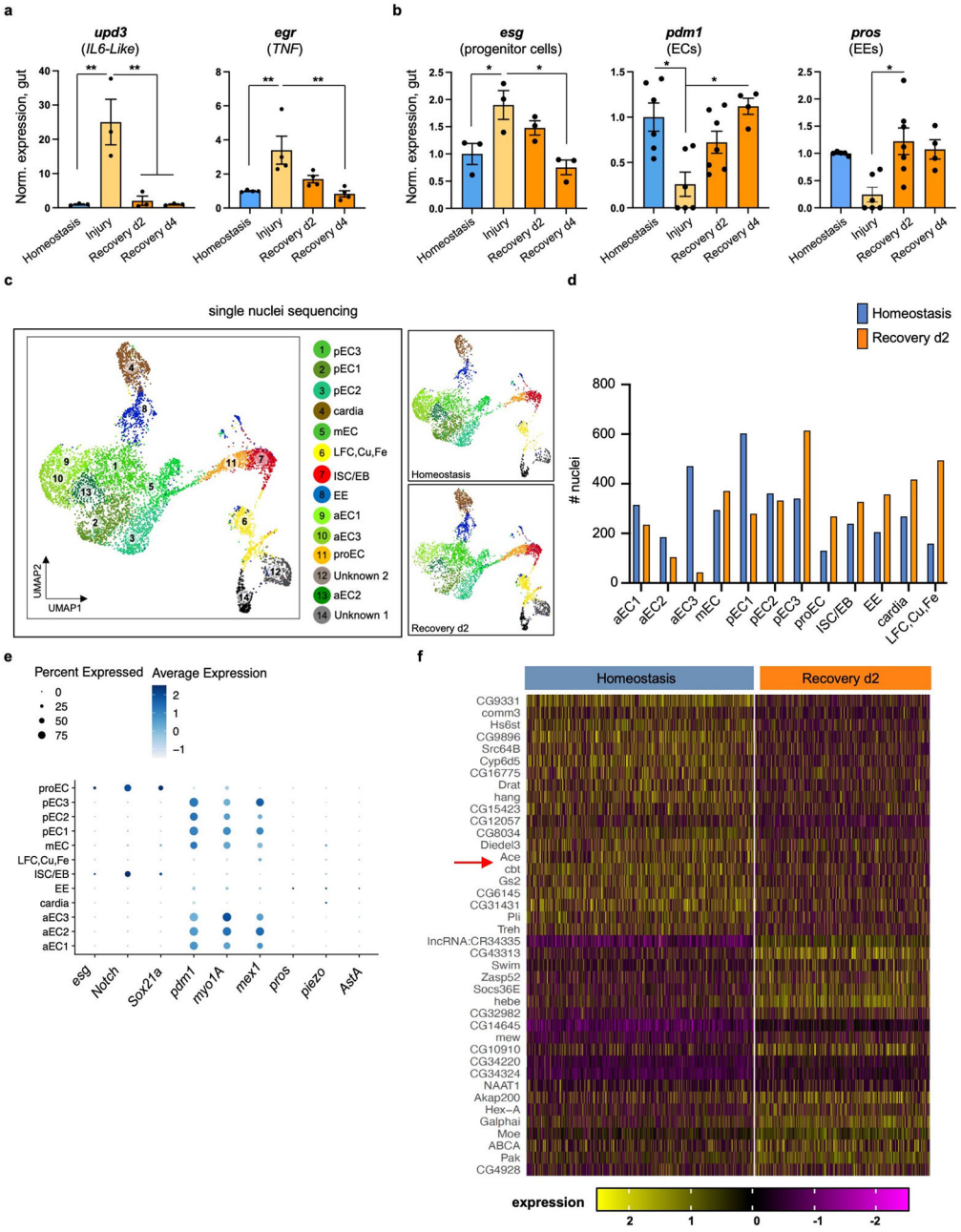

Ext. Data Fig.1 |. *Ace* is downregulated during recovery.

a, Expression levels of conserved inflammatory cytokines (*unpaired-3*/*upd-3* and *eiger*/*egr*) in guts of *Ore R* flies undergoing DSS-induced repair. Normalized to Homeostasis. n=3 biologically independent samples per condition. Tukey's one-way Anova: p=0.0046 (*upd3*: Hom. vs Injury & Injury vs Rec. d4), p=0.0061(*upd3*: Injury vs Rec. d2), p=0.0096 (*egr*: Hom. vs Injury), p=0.006 (Injury vs Rec. d4). **b,** Expression levels of markers for PCs (*escargot*, *esg*), ECs (*pdm1*), EEs (*prospero*, *pros*) in guts of *Ore R* flies undergoing DSS-induced repair. Normalized to Homeostasis. Homeostasis: n=3 (*esg*), n=6 (*pdm1*),

Author Manuscript Author Manuscript Author Manuscript Author Manuscript

n=5 (*pros*) biologically independent samples. Injury: n=3 (*esg*), n=6 (*pdm1*), n=6 (*pros*) biologically independent samples. Rec. d2: n=3 (*esg*), n=7 (*pdm1*, *pros*) biologically independent samples. Rec. d4: n=3 (*esg*), n=4 (*pdm1*, *pros*) biologically independent samples. Tukey's one-way Anova: p=0.0393 (Hom. vs Injury, *esg*), p=0.0112 (Injury vs Rec. d4, *esg*). Dunn's Kruskal-Wallis test: p=0.0384 (Hom. vs Injury, *pdm1*), p=0.0227 (Injury vs Rec. 4, *pdm1*), p=0.0157 (Injury vs Rec. d2, *pros*). **c,** Annotated gut cell type clusters of *Ore R* flies after snRNAseq, visualized with UMAP (n= total of 8073 nuclei). **d,** Graph depicting the number of gut nuclei recovered per cluster and per condition after snRNAseq of *Ore R* flies (n=total of 7411 nuclei in gut clusters). **e,** Dot plot per snRNAseq gut cluster illustrating the average expression (blue color range) and percent of expression (dot size) of marker genes for ECs (*pdm1*, *myo1A*, *mex1*), EEs (*pros*, *piezo*, *AstA*) and for PCs (*esg*, *Notch*, *Sox21a*) [PCs: ISC/EB and proEC]. (n=total of 7411 gut nuclei). **f,** Heatmap of significantly upregulated and downregulated genes in EC clusters (S. Table 1-2) after snRNAseq (n= total of 4547 nuclei in EC clusters). Red arrow: *Acetylcholinesterase* (*Ace*). *: 0.05>p>0.01, **: 0.01>p>0.001. Data are presented as mean values ± SEM.

Author Manuscript Author Manuscript Author Manuscript Author Manuscript

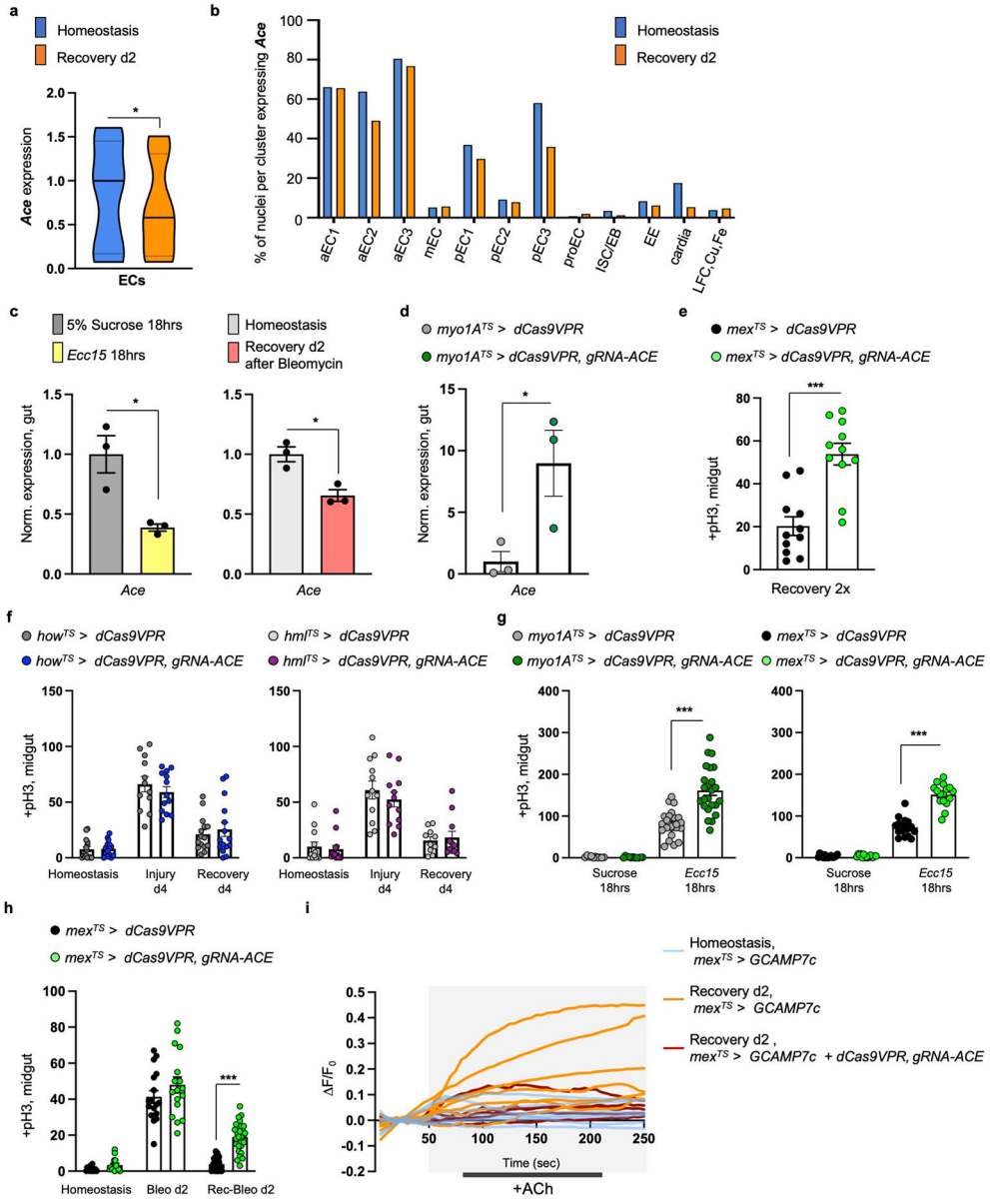

Ext. Data Fig.2 |. ACh sensitivity is required for recovery.

a, Violin plot illustrating the mean expression of *Ace* per condition in EC clusters after snRNAseq *of Ore R* flies (p=0.0364). n= 4547 nuclei in EC clusters. Statistics: two-tailed negative binomial exact test, adjusted with Benjamini-Hochberg procedure. Violin plot: median, 1st and 3rd quartile. **b,** Graph depicting percentage of nuclei expressing *Ace* per snRNAseq gut cluster and condition (n=7411 gut nuclei). **c,** Expression levels of *Ace* in *Ore R* guts after 18hrs of *Ecc15* bacterial infection (yellow) or 2 days after Bleomycin-injury (pink) compared to unchallenged guts (5% sucrose: grey, homeostasis: light grey). n=3 biologically independent samples per condition. two-tailed t-test: p=0.0179 (Suc. vs *Ecc15*), p=0.0121 (Hom. vs Bleo). **d,** Validation of *ACE* overexpression using CRISPR-OE .n=3 biologically independent samples per genotype. two-tailed t-test: p=0.0461. **e,** Mitotic division counts of proliferating ISCs with anti-pH3 from midgut of control (*mex^{TS} >*

Author Manuscript Author Manuscript Author Manuscript Author Manuscript

dCas9VPR) and flies with conditional *Ace* overexpression (*mex^{TS} > dCas9VPR, gRNA-Ace*) in ECs during Recovery 2x (like Fig.1f). n=11 guts per genotype examined over 2 independent experiments. two tailed Mann-Whitney test: p=0.0001. **f,** pH3+ counts from midgut of control (*how^{TS} > dCas9VPR, hml^{TS} > dCas9VPR*) and flies with conditional *Ace* overexpression in the visceral muscle (*how^{TS} > dCas9VPR, gRNA-Ace*) and in hemocytes (immune cells, *hml^{TS} > dCas9VPR, gRNA-Ace*). Conditions like Fig. 1e. Two-way Anova. *how^{TS}>dCas9VPR*: n=15(Hom, Rec.d4), n=12(Injury) guts; *how^{TS}>dCas9VPR,gRNA-Ace*: n=15(Hom, Rec.d4), n=13 (Injury) guts; *hml^{TS} > dCas9VPR*: n=13(Hom.), n=12(Injury), n=10(Rec. d4) guts, *hml^{TS}>dCas9VPR,gRNA-Ace*: n=14(Hom.), n=12 (Injury), n=11(Rec. d4) guts, examined over 3 independent experiments. **g,** pH3+counts from midgut of control (*myo1A^{TS}> dCas9VPR, mex^{TS} > dCas9VPR*) and flies with conditional *Ace* overexpression (*myo1A^{TS}> dCas9VPR, gRNA-Ace* and *mex^{TS} > dCas9VPR, gRNA-Ace*) in ECs after 18hrs of 5% sucrose feeding or 18hrs of *Ecc15* oral infection (29°C). *myo1A^{TS}> dCas9VPR*: n=10(Suc.), n=23 (*Ecc15*) guts; *myo1A^{TS}>dCas9VPR,gRNA-Ace*: n=11(Suc.), n=24(*Ecc15*) guts; *mex^{TS}> dCas9VPR*: n=16(Suc.), n=17(*Ecc15*) guts; *mex^{TS}>dCas9VPR, gRNA-Ace*: n=15(Suc.), n=16 (*Ecc15*) guts, examined over 2 independent experiments. Tukey's one-way Anova. **h,** pH3+ counts from *mex^{TS} > dCas9VPR* and *mex^{TS} > dCas9VPR, gRNA-Ace* guts during Homeostasis, 2 days feeding with Bleomycin (Bleo d2) and 2 days recovery after Bleomycin (Rec-Bleo d2) at 29°C. *mex^{TS}> dCas9VPR*: n=15(Hom.), n=17(Bleo.), n=32 (Rec.) guts; *mex^{TS}>dCas9VPR, gRNA-Ace*: n=16(Hom.), n=17 (Bleo.), n=29 (Rec.) guts, examined over 3 independent experiments. Tukey's one-way Anova. **i,** Relative fluorescence intensity ($\Delta F/F_0$) per frame (5 seconds per frame) and per genotype of individual guts as described in Fig. 1g. *: 0.05>p>0.01, ***: p<0.001. Data are presented as mean values ± SEM.

Author Manuscript Author Manuscript Author Manuscript Author Manuscript

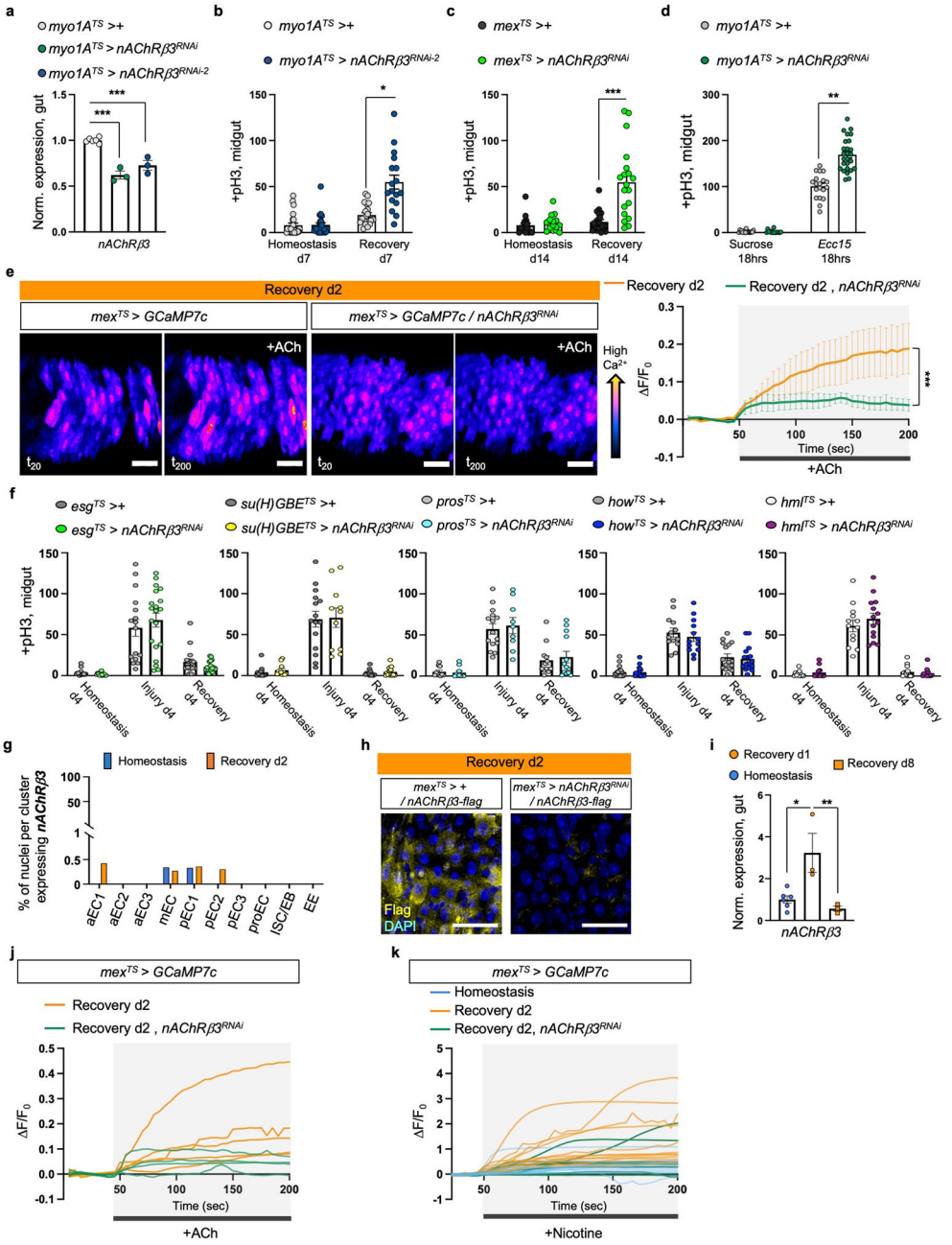

Ext. Data Fig.3 | nAChRβ3 is required in ECs for recovery.

a, *nAcRβ3*$^{\text{RNAi}}$ validation. n=6 (control), n=3 (*nAChRβ3*^{RNAi} , *nAChRβ3*$^{RNAi\text{-}2}$) biologically independent samples. Statistics: Dunnett's one-way Anova. **b,** pH3+ counts from control (*myo1A*^{TS}*>+*) guts and when *nAChRβ3* is reduced in ECs (*myo1A*^{TS}*>nAChRβ3*$^{RNAi\text{-}2}$). Recovery d7: 7 days standard food (29°C) after 4 days DSS-feeding (23°C). Homeostasis d7: 7 days standard food (29°C). p= 0.0496 (Dunn's Kruskal-Wallis test). *myo1A*^{TS}*>+*: n=23(Hom.), n=20(Rec. d7) guts; *myo1A*^{TS}*>nAChRβ3*$^{RNAi\text{-}2}$: n=23(Hom.), n=17(Rec. d7) guts, examined over 3 independent experiments. **c,** pH3+ counts from *mex*^{TS}*>+* and *mex*^{TS}*>nAChRβ3*^{RNAi} guts. Recovery d14: 14 days standard food (29°C) after 4 days of DSS-feeding (23°C). Homeostasis d14: 14 days standard

Author Manuscript Author Manuscript Author Manuscript Author Manuscript

food (29°C). p= 0.0007(Kruskal-Wallis test). *mex^{TS}>+* : n=16(Hom.), n=20(Rec. d14) guts; *mex^{TS}>nAChRβ3^{RNAi}*: n=16(Hom.), n=19(Rec. d14) examined over 3 independent experiments. **d,** pH3+ counts from *myo1A^{TS}>+* and *myo1A^{TS} >nAChRβ3^{RNAi}* guts after *Ecc15* oral infection and after 5% sucrose feeding. Conditions like Ext. Data Fig.2g. p= 0.0099 (Dunn's Kruskal-Wallis test). *myo1A^{TS}>+* : n=17 (Suc.), n=19 (*Ecc15*) guts; *myo1A^{TS} >nAChRβ3^{RNAi}* n=15 (Suc.), n=26 (*Ecc15*) guts examined over 3 independent experiments. **e,** Representative color-coded sequential frames before (fr_{20}) and after (fr_{200}) ACh administration from control (*mex^{TS} > GCAM7c*) and *mex^{TS} > GCAM7c +nAChRβ3^{RNAi}* midguts (Like in Fig. 1g). scale bar: 25μm. Accompanying graph: average relative fluorescence intensity ($\Delta F/F_0$) per frame (5 seconds per frame) and per genotype. n=4 (control), n=5 (*nAChRβ3^{RNAi}*) guts examined over 2 independent experiments (two-way Anova). Individual $\Delta F/F_0$ per gut on Ext. Data Fig.3j. **f,** pH3+ counts from control and when reducing *nAcRβ3* in PCs (*esg^{TS}>nAChRβ3^{RNAi}*), EBs (*su(H)GBE^{TS}>nAChRβ3^{RNAi}*), EEs (*pros^{TS}> nAChRβ3^{RNAi}*), visceral muscle (*how^{TS} > nAChRβ3^{RNAi}*) and hemocytes (*hml^{TS}> nAChRβ3^{RNAi}*). Conditions like Fig. 1e. Statistics: Sidak's two-way Anova. *esg^{TS}>+* : n=16 (Hom., Injury) n=17 (Rec.) guts; *esg^{TS}>nAChRβ3^{RNAi}*: n=14(Hom.), n= 20(Injury), n=18(Rec) guts, over 2 independent experiments. *Su(H)GBE^{TS}>+* : n=16(Hom.), n=15 (Injury), n=13 (Rec.) guts; *Su(H)GBE^{TS}>nAChRβ3^{RNAi}*: n=11(Hom., Injury), n=15(Rec) guts examined over 2 independent experiments. *pros^{TS}>+* : n=10 (Hom.), n=15(Injury), n=12(Rec.) guts; *pros^{TS}>nAChRβ3^{RNAi}*: n=10(Hom.), n=9(Injury), n=13(Rec) guts examined over 2 independent experiments. *how^{TS}>+* : n=20(Hom.), n=13(Injury), n=16(Rec.) guts; *how^{TS}>nAChRβ3^{RNAi}*: n=19(Hom.), n=13(Injury), n=16(Rec) guts examined over 2 independent experiments. *hml^{TS}>+* : n=12(Hom.), n=13(Injury), n=14(Rec.) guts; *hml^{TS}>nAChRβ3^{RNAi}*: n=12(Hom.), n=14(Injury), n=13(Rec) guts examined over 2 independent experiments. **g,** Graph depicting percentage of nuclei expressing *nAChRβ3* per snRNAseq gut cluster (n=7411 gut nuclei). **h,** nAChRβ3-flag validation: Midgut expressing nAChRβ3-flag (*mex^{TS}> +/nAChRβ3-flag*) and when knocking down *nAChRβ3* in ECs (*mex^{TS}>nAChRβ3^{RNAi}/nAChRβ3-flag).* anti-Flag: nAChRβ3-flag (yellow). DAPI: nuclei (blue). Images are representative of 2 independent experiments with similar results. scale bar: 25μm. **i,** *nAChRβ3* expression levels in *Ore R* guts. Tukey's one-way Anova: p= 0.0104(Hom. vs Rec. d1), p=0.0085(Rec. d1 vs Rec. d8). n= 6 (Hom.), n=3(Rec. d1, Rec. d8) biologically independent samples. **j-k,** Relative fluorescence intensity ($\Delta F/F_0$) per frame (5 seconds per frame) and genotype of each gut as described in Ext. Data Fig.3e and Fig. 2g, respectively. *: 0.05>p>0.01, **: 0.01<p<0.001, ***: p<0.001. Data are presented as mean values ± SEM.

Author Manuscript Author Manuscript Author Manuscript Author Manuscript

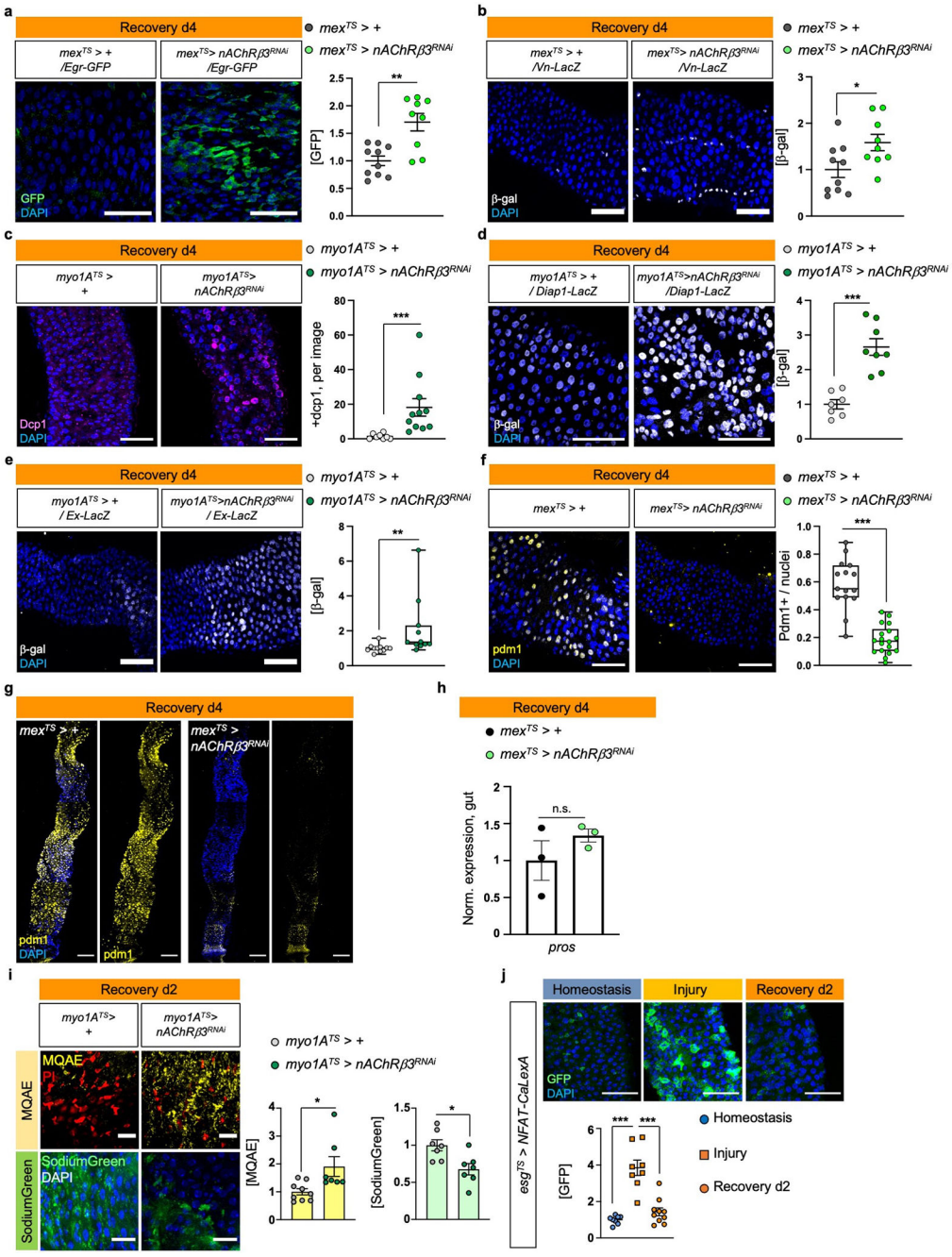

Ext. Data Fig.4 |. nAChRβ3 promotes EC maturation.

a, Representative image of posterior midgut from control (*mex*^{TS}*>+/Egr-GFP*) flies and when *nAChRβ3* is reduced in ECs (*mex*^{TS}*>nAChRβ3*^{RNAi}*/ Egr-GFP*) together with the protein trap Egr-GFP (anti-GFP, green). Accompanying graph: fluorescence fold change per image. n=10 (control), n=9 (*nAChRβ3*^{RNAi}) guts examined over 2 independent experiments. Statistics: two-tailed Mann-Whitney test, p=0.0057. Conditions like Fig.1e. scale bar: 50μm. **b,** Representative images of posterior midguts from control (*mex*^{TS}*>+/Vn-LacZ*) and when *nAChRβ3* is reduced in ECs (*mex*^{TS}*> nAChRβ3*^{RNAi}*/Vn-LacZ*) together with the *Vn-LacZ* reporter (anti-β-gal, white). Accompanying graph: fluorescence fold change per image. n=10

Author Manuscript Author Manuscript Author Manuscript Author Manuscript

(control), n=9 (*nAChRβ3*^{RNAi}) guts examined over 2 independent experiments. Conditions like Fig.1e. Statistics: two-tailed t-test, p=0.0279. scale bar: 50μm. **c,** Representative images of posterior midguts from *myo1A*^{TS}*>+* and *myo1A*^{TS}*> nAChRβ3*^{RNAi} flies stained with anti-Dcp1: cell death (pink). Conditions like Fig.1e. Accompanying graph: Dcp1+ cells per image. n=8 (control), n=11 (*nAChRβ3*^{RNAi}) guts examined over 2 independent experiments. Statistics: two-tailed Mann-Whitney test. scale bar: 50μm. **d,** Representative images of posterior midguts from control (*myo1A*^{TS}*>+/Diap1-LacZ*) and when knocking down *nAChRβ3* in ECs (*myo1A*^{TS}*> nAChRβ3*^{RNAi}*/Diap1-LacZ*) together with *Diap1-LacZ* (Yki target gene, anti-β-gal: white). Conditions like Fig.1e. Accompanying graph: fluorescence fold change per image. n=7 (control), n=8 (*nAChRβ3*^{RNAi}) guts examined over 2 independent experiments. Statistics: two-tailed t-test. scale bar: 50μm. **e,** Representative images of posterior midgut from control (*myo1A*^{TS}*>+/Ex-LacZ*) and when *nAChRβ3* is reduced in ECs (*myo1A*^{TS}*> nAChRβ3*^{RNAi} */Ex-LacZ*) together with *Ex-LacZ* (Yki target gene, anti-β-gal: white). Conditions like Fig.1e. Boxplot: fluorescence fold change per image (median, 1st and 3rd quartile, whiskers: minimum maximum values). n=11 guts per genotype examined over 2 independent experiments. Statistics: two-tailed Mann-Whitney test, p=0.0014. scale bar: 50μm. **f-g,** Representative images from posterior midgut of *mex*^{TS}*>+* and *mex*^{TS}*> nAChRβ3*^{RNAi} flies stained with anti-pdm1: EC (yellow). Conditions like Fig.1e. Boxplot: pdm1+ cells over total nuclei per image (median, 1st and 3rd quartile, whiskers: minimum maximum values). n=15 (control), n=18 (*nAChRβ3*^{RNAi}) guts examined over 3 independent experiments. Statistics: two-tailed t-test. scale bars: 50μm(f),100μm(g). **h,** *Pros* expression levels. n=3 biologically independent samples per genotype. Statistics: two-tailed t-test. **i,** Representative images of posterior midgut assayed with MQAE dye (intracellular Cl^- via diffusion-limited collisional quenching, yellow) and SodiumGreen dye (intracellular Na^+, green) from control *myo1A*^{TS}*>+* and *myo1A*^{TS}*>nAChRβ3*^{RNAi} flies. PI: nuclei (Propidium Iodide, red). See Methods for conditions. Accompanying graphs: fluorescence fold change per image. n= 9 (control/MQAE), n=7 (*nAChRβ3*^{RNAi}/MQAE) guts, n=7 (SodiumGreen per genotype) guts examined over 2 independent experiments per dye. Statistics: p=0.0115 (two tailed Mann-Whitney test/ MQAE), p=0.0103 (two-tailed t-test/SodiumGreen). scale bar: 20μm. **j,** Representative images from posterior midgut with PCs expressing *NFAT-CaLexA* (*esg*^{TS}*>NFAT-CaLexA*). anti-GFP: Ca^{2+} (green). *NFAT-CaLexA* was expressed for 2 days (29°C) per condition. Accompanying graph: fluorescence fold change per image. n= 8 (Hom., Injury), n=10 (Rec. d2) guts examined over 2 independent experiments (Tukey's one-way Anova). scale bar: 50μm. *: 0.05>p>0.01, **: 0.01<p<0.001, ***: p<0.001. n.s.: non-significant. Data are presented as mean values ± SEM.

Author Manuscript Author Manuscript Author Manuscript Author Manuscript

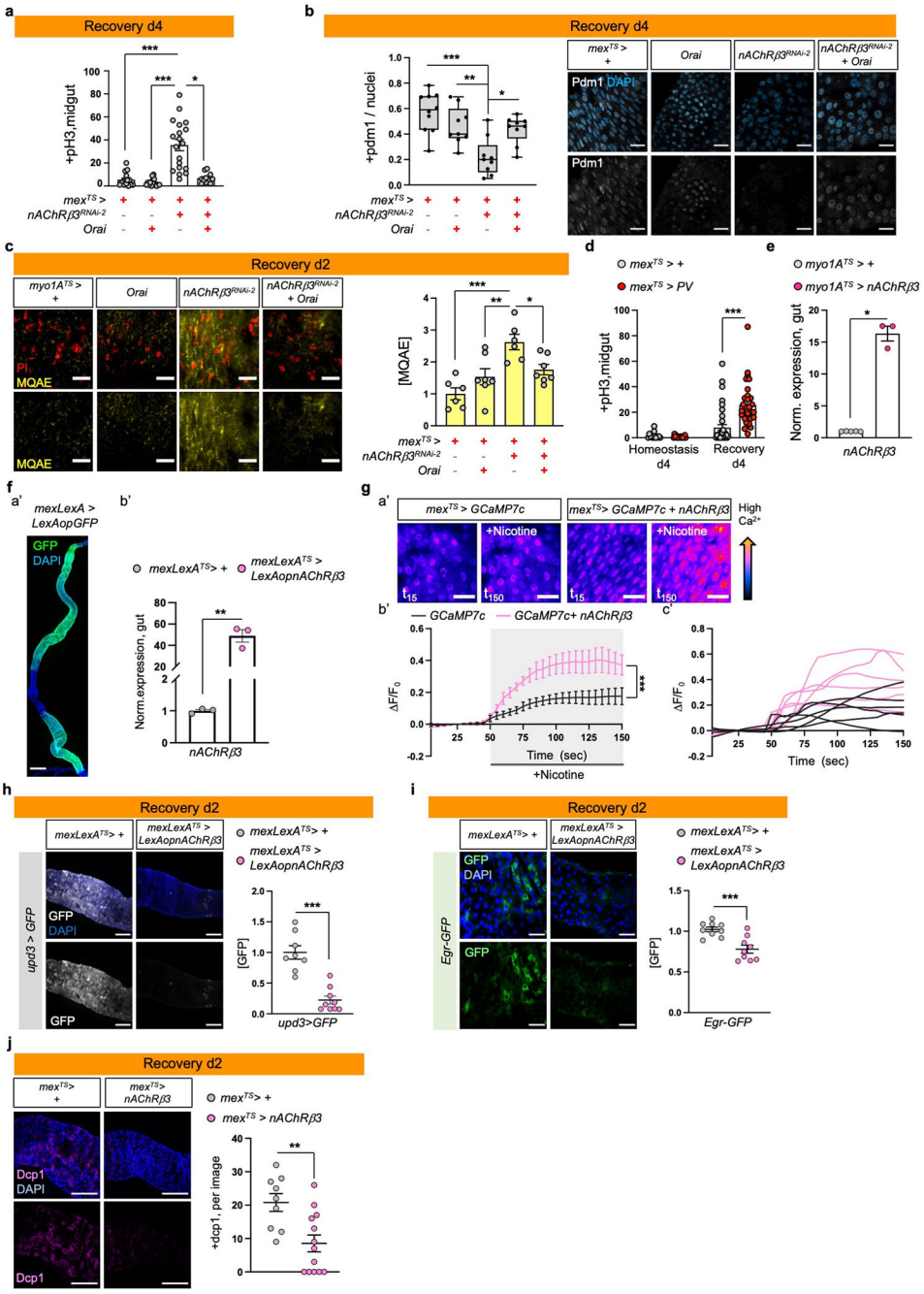

Ext. Data Fig.5 |. nAChRβ3-mediated Ca^2 promotes recovery.

a, pH3+ counts of control (*mex^{TS}>+*), guts with Orai (Ca^{2+} channel) overexpressed in ECs (*mex^{TS}>Orai*), *nAChRβ3* reduced in ECs (*mex^{TS}>nAChRβ3^{RNAi-2}*) and combined (*mexA^{TS}>nAChRβ3^{RNAi-2}+ Orai*) during Recovery d4 (Like Fig.1e). n=15 (*mex^{TS}>+*), n=19 (*mex^{TS}>nAChRβ3^{RNAi-2}*), n=16 (*mex^{TS}>Orai*), n=11(*mexA^{TS}>nAChRβ3^{RNAi-2}+ Orai*) guts examined over 2 independent experiments. Statistics: Dunn's Kruskal-Wallis test, p=0.013 (*nAChRβ3^{RNAi-2}* vs *nAChRβ3^{RNAi-2}+ Orai*). **b,** Representative images of posterior midgut of flies as in Ext. Data Fig.5a. anti-pdm1: ECs (grey). Boxplot: pdm1+ cells over total nuclei per image (median, 1st and 3rd quartile, whiskers: minimum maximum values).

Author Manuscript Author Manuscript Author Manuscript Author Manuscript

n=10 (control), n=9 (*nAChRβ3^{RNAi-2}*, *Orai nAChRβ3^{RNAi-2}+ Orai* guts) guts examined over 2 independent experiments. Statistics: Tukey's one-way Anova, p=0.0048 (*nAChRβ3^{RNAi-2}* vs *Orai*), p=0.0144 (*nAChRβ3^{RNAi-2}* vs *nAChRβ3^{RNAi-2}+ Orai*). scale bar: 25μm. **c,** Representative images of posterior midguts assayed with MQAE (like Ext. Data Fig.4i) of *myo1A^{TS}>+*, *myo1A^{TS}>Orai*, *myo1A^{TS}>nAChRβ3^{RNAi-2}* and *myo1A^{TS}>nAChRβ3^{RNAi-2} + Orai* flies. Accompanying graph: fluorescence fold change per image. n=6 (*myo1A^{TS}>+*), n=6 (*myo1A^{TS}>nAChRβ3^{RNAi-2}*), n=7(*myo1A^{TS}>Orai*), n=7 (*myo1A^{TS}>nAChRβ3^{RNAi-2} +Orai*) guts examined over 2 independent experiments. Statistics: Tukey's one-way Anova, p=0.0002 (control vs *nAChRβ3^{RNAi-2}*), p=0.0084 (*Orai* vs *nAChRβ3^{RNAi-2}*), p=0.0441 (*nAChRβ3^{RNAi-2}* vs *Orai + nAChRβ3^{RNAi-2}*). scale bar: 25μm. **d,** pH3+ counts from control (*mex^{TS}>+*) and flies overexpressing parvalbumin in ECs (*mex^{TS}>PV*). Conditions like Fig. 1e. Control: n=14 (Hom.), n=37 (Rec.d4) guts, *mex^{TS}>PV*: n=17 (Hom.), n=30 (Rec.d4) guts examined over 3 independent experiments. Statistics: Dunn's Kruskal-Wallis test. **e,** Validation of UAS-*nAcRβ3*. n=6 (control), n=3 (*myo1A^{TS}> nAcRβ3*) biologically independent samples. Statistics: two-tailed Mann-Whitney test, p=0.0357. **f,** Validation of a': *mexLexA* (*mexLexA::GAD*), scale bar: 200μm. Image is representative of 2 independent experiments with similar results; b': *LexAopnAChRβ3*. n= 3 biologically independent samples per genotype. Statistics: two-tailed t-test, p=0.0012. **g,** a': Representative color-coded sequential frames of *mex^{TS}>GCAM7c* and *mex^{TS}>GCAM7c+nAChRβ3* guts before (t_{15}) and after (t_{150}) nicotine administration. b': average relative fluorescence intensity ($\Delta F/F_0$) per frame (5 seconds per frame) and genotype. Conditions: 2 days standard food (29°C). N=6 guts per genotype examined over 2 independent experiments. c': relative fluorescence intensity of each gut. Statistics: two-way Anova. scale bar: 25μm. **h,** Representative images of posterior midguts from control (*mexLexA^{TS}>+/upd3>GFP*) and when *nAChRβ3* is overexpressed in ECs (*mexLexA^{TS}> LexAopnAChRβ3 /upd3>GFP*) together with *upd3-Gal4* driving *UAS-GFP* (anti-GFP, white). Conditions like Fig. 3g. Accompanying graph: fluorescence fold change per image. n=8 (control), n=9 (*mexLexA^{TS}> LexAopnAChRβ3*) guts examined over 2 independent experiments. Statistics: two-tailed Mann-Whitney test, p=0.0002. scale bar: 100μm. **i,** Representative images of posterior midguts from *mexLexA^{TS}>+/Egr-GFP* and *mexLexA^{TS}>LexAopnAChRβ3/Egr-GFP* flies (anti-GFP, green). Conditions like Fig. 3g. Accompanying graph: fluorescence fold change per image. n=9 guts per genotype examined over 2 independent experiments. Statistics: two-tailed t-test, p=0.0006. scale bar: 25μm. **j,** Representative images of posterior midguts from control (*mex^{TS}>+*) and *mex^{TS}>nAChRβ3* flies stained with anti-Dcp1(pink). Conditions like Fig. 3g. Accompanying graph: Dcp1+ cells per image. n=9 (control), n=13 (*mex^{TS}>nAChRβ3*) guts per genotype examined over 2 independent experiments. Statistics: two-tailed Mann-Whitney test, p=0.0064. scale bar: 100μm. DAPI: nuclei (blue). PI: nuclei (Propidium iodide, red). *: 0.05>p>0.01, **: 0.01<p<0.001, ***: p<0.001. Data are presented as mean values ± SEM.

Author Manuscript Author Manuscript Author Manuscript Author Manuscript

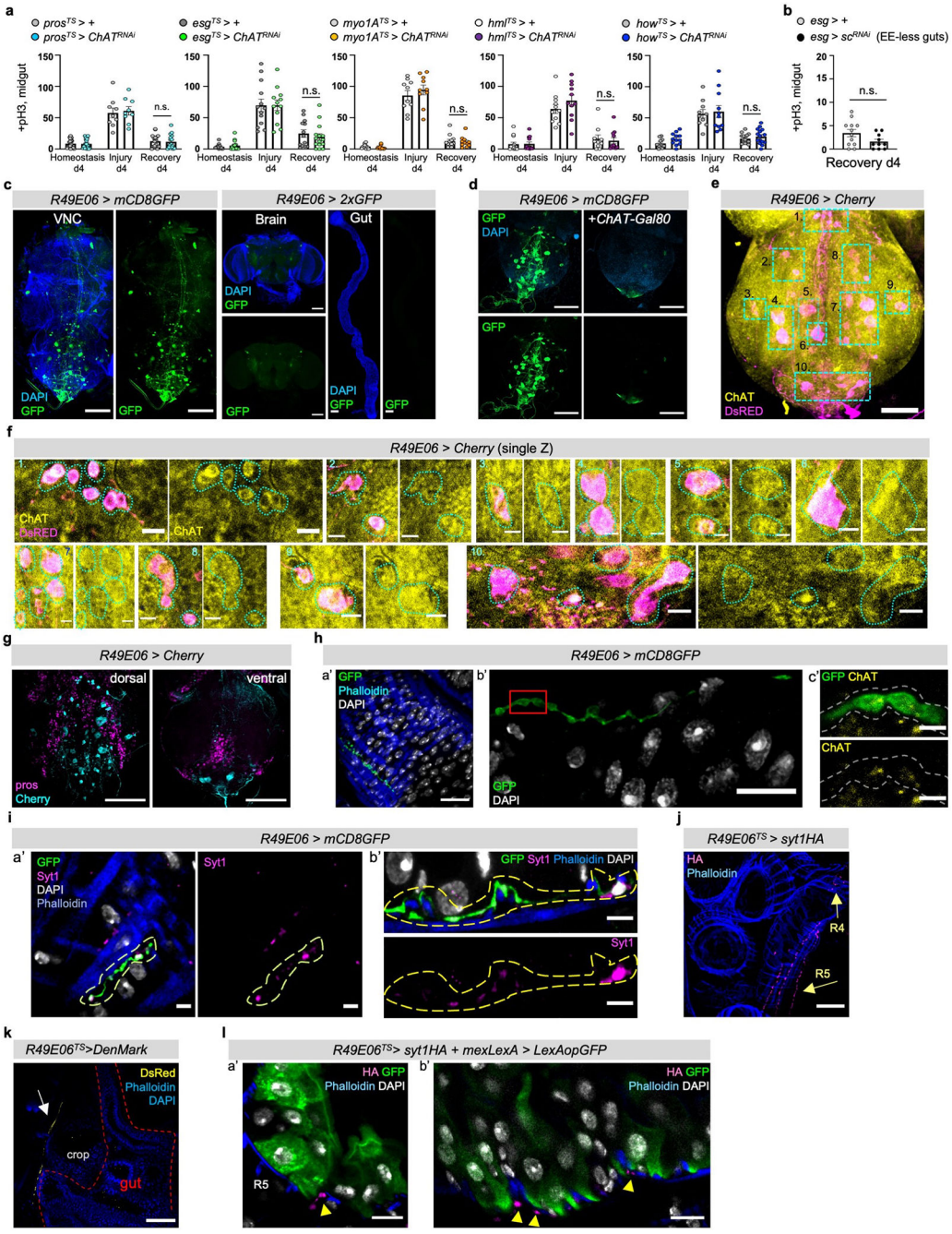

Ext. Data Fig.6 | R49E06-neurons innervate the gut.

a, pH3+ counts from control and from flies with conditional reduction of *ChAT* (*Choline Acetyltransferase)* in EEs (*pros*^{TS}>), PCs (*esg*^{TS}>), ECs (*myo1A*^{TS}>), hemocytes (*hml*^{TS}>), visceral muscle (*how*^{TS}>). Conditions like Fig.1e. *pros*^{TS}>+: n=20 (Hom.), n=9 (Injury), n=18 (Rec.) guts, *pros*^{TS}>*ChAT*^{RNAi}: n=20 (Hom.), n=9 (Injury), n=16 (Rec.) guts; *esg*^{TS}>+: n=13 (per condition) guts, *esg*^{TS}>*ChAT*^{RNAi}: n=15 (Hom.), n=12 (Injury), n=15 (Rec.) guts; *myo1A*^{TS}>+: n=11(Hom.), n=10 (Injury), n=12 (Rec.) guts, *myo1A*^{TS}>*ChAT*^{RNAi}: n=12 (Hom.), n=10 (Injury), n=11 (Rec.) guts; *hml*^{TS}>+: n=13 (Hom.), n=11 (Injury), n=10 (Rec.) guts, *hml*^{TS}>*ChAT*^{RNAi}: n=12 (Hom.), n=11

Author Manuscript Author Manuscript Author Manuscript Author Manuscript

(Injury), n=11 (Rec.) guts; *how*^{TS}*>+*: n=11(Hom.), n=10 (Injury), n=15 (Rec.) guts, *how*^{TS}*>ChAT*^{RNAi}: n=12 (Hom.), n=11 (Injury), n=15 (Rec.) guts examined over two independent experiments per cell type. Statistics: Sidak's two-way Anova. **b,** pH3+counts from control (*esg>+*) and from flies without EEs (*esg>sc*^{RNAi}). n= 12 (control), n= 10 (*esg>sc*^{RNAi}) guts examined over 2 independent experiments. Statistics: two-tailed t-test. **c,** VNC (adult Ventral Nerve Cord), brain, and gut from *R49E06>mCD8GFP* and *R49E06>2xEGFP* flies. Images are representative of 3 independent experiments with similar results. anti-GFP: green. scale bar: 100μm. **d,** Posterior VNC from *R49E06>mCD8GFP* flies and together with the cholinergic repressor *R49E06>mCD8GFP/ ChAT-Gal80*. anti-GFP: green. scale bar: 100μm. Images are representative of 2 independent experiments with similar results. **e-f,** Z-stack (e) and single Z-planes (f) from posterior VNC of *R49E06>6xmCherry*. anti-DsRed: magenta, anti-ChAT: yellow, numbered squares: ChAT+R49E06-neurons. scale bar: 50μm(e), 10μm (f). Image (e) is representative of 2 independent experiments with similar results. **g,** Posterior VNC from *R49E06>6xmCherry*. anti-pros: magenta, anti-DsRed: cyan. Ventral and dorsal from same stack. scale bar: 100μm. Images are representative of 2 independent experiments with similar results. **h,** R49E06-innervations (anti-GFP, green) in midguts of *R49E06>mCD8GFP* flies; a': R4, Homeostasis, b': R5, Recovery d2. Red square: domain of R49E06-innervation in c. c': R49E06-innervation (grey line), anti-ChAT: yellow. scale bar: 20μm(h-a'), 10μm (h-b'), 2μm (h-c'). Images are representative of 2 independent experiments with similar results per condition. **i,** a': innervated R4, b': R5 from *R49E06>mCD8GFP* flies during Homeostasis. anti-GFP: R49E06-innervations (green), anti-Syt1: synaptic-vesicle marker (magenta). Yellow dots: Syt1+ boutons across innervations. scale bar: 4μm. Images are representative of 2 independent experiments with similar results. **j,** *R49E06*^{TS}*>syt1HA* fly abdomen during Recovery d2. Yellow arrows: R49E06-innervations (anti-HA, magenta). scale bar: 50μm. Images are representative of 3 independent experiments with similar results. **k,** Fly abdomen with DenMarK expressed in R49E06-projections (*R49E06*^{TS}*>DenMark*) during Recovery d2 (like Fig. 4a). anti-DsRed: DenMark (yellow). White arrow: DenMark-expressing ARCEN-projections, Dotted red line: gut. scale bar: 100μm. Images are representative of 2 independent experiments with similar results. **l,** R5 from *R49E06*^{TS}*>syt1HA+mexLexA>6xLexAopGFP* (a') and *R49E06*^{TS}*>syt1HA+mexLexA>LexAopGFP* (b') flies during Recovery d2. Yellow arrowheads: R49E06-innervations carrying the presynaptic marker syt1HA (anti-HA, magenta) near ECs (anti-GFP, green). Images are representative of 3 independent experiments with similar results. scale bar: 10μm. Phalloidin: muscle (blue). DAPI: nuclei (blue or white); n.s.: non-significant. Data are presented as mean values ± SEM.

Author Manuscript Author Manuscript Author Manuscript Author Manuscript

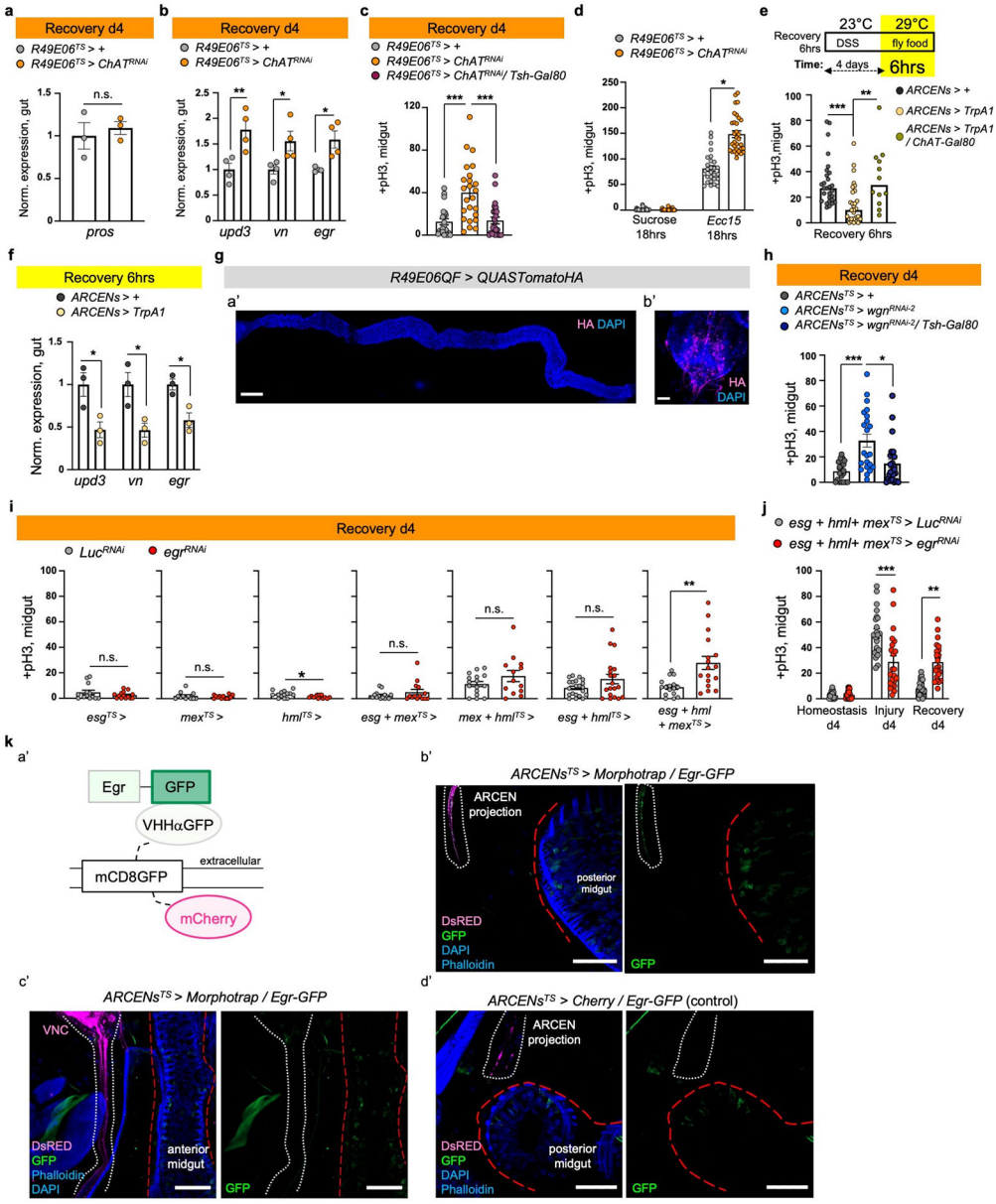

Ext. Data Fig.7 |. Egr-ARCENs signaling promotes recovery.

a-b, *Pros, upd3, vn, egr* expression levels from control (*R49E06^{TS}>+*) guts and guts after knocking down *ChAT* in R49E06-neurons (*R49E06^{TS}>ChAT^{RNAi}*). Conditions like Fig. 1e. a: n=3 biologically independent samples. b: n=4 biologically independent samples. Normalized to *R49E06^{TS}>+*. Statistics: (a) two-tailed t-test, (b) Sidak's two-way Anova: p=0.0038 (*upd3*), p=0.0412 (*vn*), p=0.0298(*egr*). **c,** pH3+ counts from *R49E06^{TS}>+* (control), *R49E06^{TS}>ChAT^{RNAi}* flies and flies co-expressing the VNC repressor (*R49E06^{TS}>ChAT^{RNAi}/Tsh-Gal80*). n= 21 (control), n=24 (*R49E06^{TS}>ChAT^{RNAi}*, *R49E06^{TS}>ChAT^{RNAi}/Tsh*-Gal80) guts examined over 3 independent experiments. Statistics: Dunn's Kruskal-Wallis test: p=0.0004. Conditions like Fig. 1e. **d,** pH3+ counts from *R49E06^{TS}>+* and *R49E06^{TS}>ChAT^{RNAi}* flies after oral *Ecc15* infection or 5% sucrose feeding (like Ext. Data Fig.2g). n=27 (*R49E06^{TS}>+* per condition), n=24

Author Manuscript Author Manuscript Author Manuscript Author Manuscript

(*R49E06^{TS}>ChAT^{RNAi}*, sucrose), n=32 (*R49E06^{TS}>ChAT^{RNAi}*, *Ecc15*) guts examined over 3 independent experiments. Statistics: Dunn's Kruskal-Wallis test: p=0.013. **e,** Experimental schematic and pH3+ counts, from control (*ARCENs>+*) files, flies with 6hrs thermo-activation of ARCENs with theTrpA1 channel (*ARCENs>TrpA1*) and when cholinergic neurons are inhibited *(ARCENs>TrpA1/ChAT-Gal80*). n=28 (control), n=29 (*ARCENs>TrpA1*), n=12 (*ARCENs>TrpA1/ChAT-Gal80*) guts examined over 2 independent experiments. Dunn's Kruskal-Wallis test: p= 0.0005(control vs *TrpA1*), p= 0.0069 (*TrpA1* vs *TrpA1/ChAT-Gal80*). **f,** *upd3*, *vn*, *egr* expression levels from *ARCENs>+* (control) and *ARCENs>TrpA1* guts. Conditions like Ext. Data Fig.7e. n=3 biologically independent samples per genotype. Normalized to *ARCENs>+*. Sidak's two-way Anova: p=0.0114 (*upd3*), p=0.0109 (*vn*), p=0.0461(*egr*). **g,** Validation of *R49E06QF*. a': gut (scale bar: 200μm), b': posterior VNC (scale bar 50μm). Images are representative of 2 independent experiments with similar results. **h,** pH3+ counts from control (*ARCENs^{TS}>+*) flies, flies with TNF receptor *wgn* reduced in ARECNs (*ARCENs^{TS}>wgn^{RNAi-2}*) and flies co-expressing the VNC repressor (*ARCENs^{TS}>wgn^{RNAi-2}/Tsh-Gal80*). Conditions like Fig.1e. n=21 (control), n=22 (*ARCENs^{TS}>wgn^{RNAi-2}*), n=25(*ARCENs^{TS}>wgn^{RNAi-2}/ Tsh-Gal80*) guts examined over 3 independent experiments. Dunn's Kruskal-Wallis: p=0.0004(control vs *wgn^{RNAi-2}*), p=0.0105(*wgn^{RNAi-2}* vs *wgn^{RNAi-2}* /Tsh-Gal80). **i,** pH3+ from control (*Luc^{RNAi}*) and flies with *egr* reduced (*egr^{RNAi}*) in PCs (*esg^{TS}>*), ECs (*mex^{TS}>*) and hemocytes (*hml^{TS}>*). Conditions like Fig.1e. *esg^{TS}*: n=13 (control), n=14 (*egr^{RNAi}*) guts examined over 2 independent experiments (two-tailed Mann-Whitney test). *mex^{TS}*: n=12 (control), n=13 (*egr^{RNAi}*) guts examined over 2 independent experiments (two-tailed Mann-Whitney test). *hml^{TS}*: n=14 (control), n=13 (*egr^{RNAi}*) guts examined over 2 independent experiments (two-tailed Mann-Whitney test, p=0.028). *esg+mex^{TS}*: n=14 guts per genotype examined over 2 independent experiments (two-tailed Mann-Whitney test). *mex+hml^{TS}*: n=16 (control), n=13 (*egr^{RNAi}*) guts examined over 2 independent experiments (two-tailed t-test). *esg+hml^{TS}*: n=21 (control), n=19 (*egr^{RNAi}*) guts examined over 3 independent experiments (two-tailed Mann-Whitney test). *esg+mex+hml^{TS}*: n=16 (control), n=19 (*egr^{RNAi}*) guts examined over 3 independent experiments (two-tailed Mann-Whitney test). **j,** pH3+ counts from *esg+hml+mex^{TS}>Luc^{RNAi}* (control) and *esg+hml+mex^{TS}>egr^{RNAi}* flies. Conditions like Fig.1e. control: n=23 (Hom.), n=22 (Injury), n=40 (Rec.) guts; *egr^{RNAi}*: n=24 (Hom.), n=22 (Injury), n=39 (Rec.) guts examined over 3 independent experiments. Statistics: Sidak's two-way Anova. **k,** a': Schematic of Egr-GFP bound to extracellular morphotrap (VHHaGFP). b'-d': Images from the abdomen (b',d') and thorax (c') of flies expressing the morhotrap in ARCENs while expressing Egr-GFP (*ARCENs^{TS}>morphotrap/ Egr-GFP*) and of control flies without the morphotrap (*ARCENs^{TS}>Cherry/Egr-GFP*). white dotted lines: ARCEN projections. red lines: midgut (b',d': posterior, c': anterior). Sectioning like Fig.4a. anti-DsRed: Morphotrap and Cherry (magenta). Anti-GFP: Egr (green), Phalloidin: muscle (blue), DAPI: nuclei (blue). Images are representative of 2 independent experiments with similar results. scale bar 50μm. n.s.: non-significant ,*: 0.05>p>0.01, **: 0.01<p<0.001, ***: p<0.001. Data are presented as mean values ± SEM.

Author Manuscript Author Manuscript Author Manuscript Author Manuscript

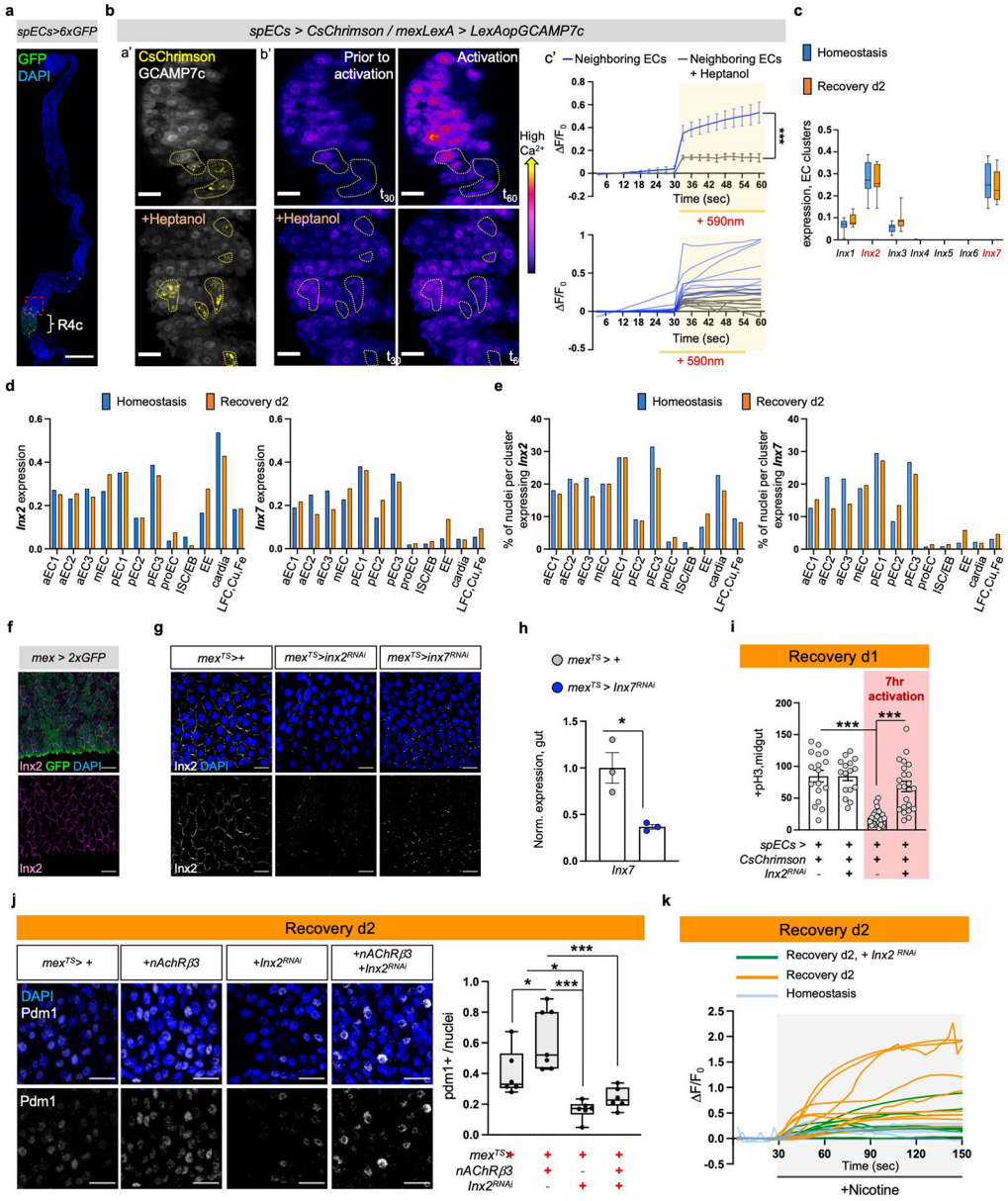

Ext. Data Fig.8 |. Ca^{2+} spreads in ECs via gap junctions.

a, Gut image with a subpopulation of ECs (spECs) expressing GFP (*spECs > 6xGFP*) that are located in R4c (between R4 and R5). anti-GFP: green. Red dotted square: area imaged in Ext. Data Fig.8b. scale bar 100μm. Image is representative of 2 independent experiments with similar results. **b,** a': Posterior midgut images of flies expressing *CsChrimson* in spECs (*spEC>CsChrimson*, yellow) while expressing *GCAMP7c* in all ECs (*mexLexA >LexAopGCAMP7c,* grey). b': Color-coded sequential frames from *spEC>CsChrimson+mexLexA > LexAopGCaMP7c* gut prior (t_{30}) and during (t_{60}) CsChrimson-activation. Lower panels: Heptanol addition (gap junction blocker). c': Fluorescence intensity ($\Delta F/F_0$) of neighboring ECs (non-expressing CsChrimson) per frame (~3 sec/frame) per condition. Upper graph: average $\Delta F/F_0$ per condition. Lower graph: individual $\Delta F/F_0$ per gut. n=10 (Neighboring ECs), n=9 (Neighboring ECs+Heptanol)

Author Manuscript Author Manuscript Author Manuscript Author Manuscript

guts examined over 3 independent experiments. Statistics: two-way Anova. yellow dots: CsChrimson-expressing ECs (spECs). scale bar 20μm. **c,** Mean expression of each *Innexin* (gap junction components) in all snRNAseq EC clusters per condition (n= 4547 nuclei in EC clusters). Boxplot: median, 1st and 3rd quartile, whiskers: minimum maximum values. **d,** Graph depicting *Inx2* and *Inx7* mean expression per snRNAseq gut cluster and condition (n=7411 gut nuclei). **e,** Graph depicting the percentage of nuclei expressing *Inx7* and *Inx2* per snRNAseq gut cluster and condition (n=7411 gut nuclei). **f,** Posterior midgut expressing GFP in ECs (*mex>2xGFP*). anti-GFP: green, anti-Inx2: magenta. scale bar 20μm. Image is representative of 2 independent experiments with similar results. **g,** Posterior midgut of control ($mex^{TS}>+$), and when conditionally knocking down *Inx2* and *Inx7* in ECs ($mex^{TS}>Inx2^{RNAi}$ and $mex^{TS}>Inx7^{RNAi}$). Conditions: 2 days standard food (29°C). anti-Inx2: grey. Images are representative of 2 independent experiments with similar results. scale bar 20μm. **h,** Validation of *Inx7* RNAi. n=3 biologically independent samples per genotype. Statistics: two-tailed t-test (p=0.0188). **i,** pH3+ counts from *spECs>CsChrimson* and *spECs>CsChrimson+* $Inx2^{RNAi}$ flies without or with 7hr opto-activation (red square) during Recovery d1. No light: n=17(*spECs>CsChrimson*), n=18 (*spECs>CsChrimson+* $Inx2^{RNAi}$) guts; Red light: n=18(*spECs>CsChrimson*), n=22 (*spECs>CsChrimson+* $Inx2^{RNAi}$) guts, examined over 3 independent experiments (Tukey's two-way Anova). **j,** Posterior midgut images from $mex^{TS}>+$, $mex^{TS}>nAcR\beta3$, $mex^{TS}>Inx2^{RNAi}$ and $mex^{TS}>nAcR\beta3+Inx2^{RNAi}$ flies. scale bar 20μm. Conditions like Fig.5f. anti-pdm1: ECs (grey). Accompanying boxplot: pdm1+ ratio (median, 1st and 3rd quartile, whiskers: minimum maximum values). n=7 ($mex^{TS}>nAcR\beta3$), n=6 ($mex^{TS}>+$, $mex^{TS}>Inx2^{RNAi}$, $mex^{TS}>nAcR\beta3+Inx2^{RNAi}$) guts, examined over 2 independent experiments. Tukey's two-way Anova: p=0.0392 ($mex^{TS}>+$ vs $mex^{TS}>nAcR\beta3$), p=0.0307 ($mex^{TS}>+$ vs $mex^{TS}>Inx2^{RNAi}$), p=0.0003 ($mex^{TS}>nAcR\beta3$ vs $mex^{TS}>nAcR\beta3+Inx2^{RNAi}$). **k,** Relative fluorescence intensity ($\Delta F/F_0$) per frame (3 seconds per frame) per genotype and per condition of individual guts as described in Fig.5g. n= 6(Hom.), n=9(Rec.),n=8($Inx2^{RNAi}$) guts examined over 2 independent experiments. DAPI: blue (nuclei). *: 0.05>p>0.01, **: 0.01<p<0.001, ***: p<0.001. Data are presented as mean values ± SEM.

Author Manuscript Author Manuscript Author Manuscript Author Manuscript

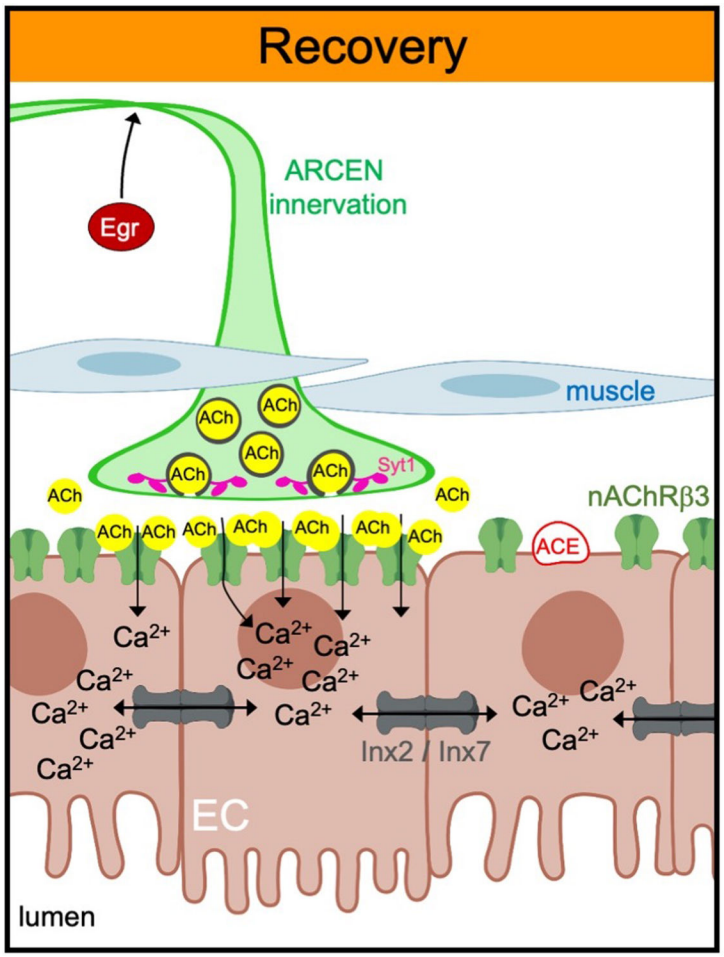

Ext. Data Fig.9 |. ARCENs trigger nAchRβ3-mediated Ca^{2+} currents in ECs to promote intestinal epithelial recovery after injury.

Model: During recovery, ECs become sensitive (*Ace* reduction) and receptive (nAChRβ3 increase) to ACh while ARCEN-innervations strengthen their Syt1+ boutons in an Egr-dependent manner. Cholinergic signaling from ARCENs to ECs triggers nAChR-mediated Ca^{2+} currents that propagate across more ECs via Inx2/Inx7 gap junctions to advance EC maturation, ion balance and transition to homeostasis. Illustration generated with BioRender.com

Supplementary Material

Refer to Web version on PubMed Central for supplementary material.

Acknowledgments:

We thank Stephanie Mohr and Justin Blau for comments on the manuscript. Confocal imaging was conducted at MicRoN Facility at Harvard Medical School, and we thank Paula Montero Llopis for advice. We thank the Cepko lab at Harvard Medical School for sharing their vibratome. We also thank Mike Levin for discussions and Hugo Bellen, Guy Tanentzapf, Kate O'Connor-Giles, Xiaohang Yang, Chris Potter, Todd R. Laverty, Gerry Rubin, Janelia FlyLight, DSHB, DRSC/TRiP, VDRC and the Bloomington Stock Center for fly lines, antibodies, and reagents. We thank Frederik Wirtz-Peitz, Sudhir Gopal Tattikota, Rich Binari and Haofan Li for help in this project and Patrick Jouandin, Pedro Saavedra, Liz Lane, David Doupé, Justin Bosch, Ben Ewen-Campen, Lucy Liu, Charles Xu, Misty

Author Manuscript Author Manuscript Author Manuscript Author Manuscript

Rose Riddle, Tyler Huycke for advice and reagents. We thank Christians Villalta and Bestgene for fly injections, Hunter Elliot and Marcelo Cicconet at the Image and Data Analysis Facility (IDAC) and Simon Norrelykke at the Image Analysis Collaboratory (IAC) at Harvard Medical School for advice on Imaris, Shahar Alon for advice on expansion microscopy, and the Biopolymers Facility and Computing facilities and PCMM Flow Cytometry Facility at Harvard Medical School. All illustrations were created with BioRender.com.

Funding:

During this study AP was a Good Ventures fellow of the Life Science Research Foundation and next was supported by the Center for the Study of Inflammatory Bowel Disease (DK043351). NP is an investigator of the Howard Hughes Medical Institute. YH, YL and AC were supported by P41GM132087 and BBSRC-NSF/BIO (DBI-2035515). YL was supported by the Finnish Cultural Foundation.

Data availability:

Raw data from main and Extended Data Figures are available in the Source Data files provided with this work. Reagents are available upon request. The snRNA-seq datasets generated in this work are publicly available in the Gene Expression Omnibus (GEO) databases under GSE218641 accession code.

GSE218641: [https://www.ncbi.nlm.nih.gov/geo/query/acc.cgi?acc=GSE218641], snRNA-seq dataset of gut from *Ore R* females flies during Homeostasis and Recovery

Single-nuclei profiling data from this study can be found at https://www.flyrnai.org/tools/rna_seq_base/web/showProject/39/plot_coord=1/sample_id=all , to allow users to query the expression of any gene of interest.

All other data are available in Figures, Ext. Data Figures and SI files (SI, SI figure, S. videos, S. Tables)

Code availability:

This study does not use any custom codes for analysis. snRNA-seq dataset were analyzed using standard Seurat pipeline.

References

1. Karin M & Clevers H Reparative inflammation takes charge of tissue regeneration. Nature 529, 307–315, doi:10.1038/nature17039 (2016). [PubMed: 26791721]
2. Miguel-Aliaga I, Jasper H & Lemaitre B Anatomy and Physiology of the Digestive Tract of Drosophila melanogaster. Genetics 210, 357–396, doi:10.1534/genetics.118.300224 (2018). [PubMed: 30287514]
3. Wessler I & Kirkpatrick CJ Acetylcholine beyond neurons: the non-neuronal cholinergic system in humans. Br J Pharmacol 154, 1558–1571, doi:10.1038/bjp.2008.185 (2008). [PubMed: 18500366]
4. Wiesner J, Kriz Z, Kuca K, Jun D & Koca J Acetylcholinesterases--the structural similarities and differences. J Enzyme Inhib Med Chem 22, 417–424, doi:10.1080/14756360701421294 (2007). [PubMed: 17847707]
5. Igaki T et al. Eiger, a TNF superfamily ligand that triggers the Drosophila JNK pathway. EMBO J 21, 3009–3018, doi:10.1093/emboj/cdf306 (2002). [PubMed: 12065414]
6. Guiza J, Barria I, Saez JC & Vega JL Innexins: Expression, Regulation, and Functions. Front Physiol 9, 1414, doi:10.3389/fphys.2018.01414 (2018). [PubMed: 30364195]
7. Snigdha K, Gangwani KS, Lapalikar GV, Singh A & Kango-Singh M Hippo Signaling in Cancer: Lessons From Drosophila Models. Front Cell Dev Biol 7, 85, doi:10.3389/fcell.2019.00085 (2019). [PubMed: 31231648]

Author Manuscript Author Manuscript Author Manuscript Author Manuscript

8. Subramanian S, Geng H & Tan XD Cell death of intestinal epithelial cells in intestinal diseases. Sheng Li Xue Bao 72, 308–324 (2020). [PubMed: 32572429]
9. Levin M Bioelectric signaling: Reprogrammable circuits underlying embryogenesis, regeneration, and cancer. Cell 184, 1971–1989, doi:10.1016/j.cell.2021.02.034 (2021). [PubMed: 33826908]
10. Hirota CL & McKay DM Cholinergic regulation of epithelial ion transport in the mammalian intestine. Br J Pharmacol 149, 463–479, doi:10.1038/sj.bjp.0706889 (2006). [PubMed: 16981004]
11. Goverse G, Stakenborg M & Matteoli G The intestinal cholinergic anti-inflammatory pathway. J Physiol 594, 5771–5780, doi:10.1113/JP271537 (2016). [PubMed: 26959627]
12. Panayidou S & Apidianakis Y Regenerative inflammation: lessons from Drosophila intestinal epithelium in health and disease. Pathogens 2, 209–231, doi:10.3390/pathogens2020209 (2013). [PubMed: 25437036]
13. Micchelli CA & Perrimon N Evidence that stem cells reside in the adult Drosophila midgut epithelium. Nature 439, 475–479, doi:10.1038/nature04371 (2006). [PubMed: 16340959]
14. Ohlstein B & Spradling A The adult Drosophila posterior midgut is maintained by pluripotent stem cells. Nature 439, 470–474, doi:10.1038/nature04333 (2006). [PubMed: 16340960]
15. Jiang H, Tian A & Jiang J Intestinal stem cell response to injury: lessons from Drosophila. Cell Mol Life Sci 73, 3337–3349, doi:10.1007/s00018-016-2235-9 (2016). [PubMed: 27137186]
16. Guo Z, Driver I & Ohlstein B Injury-induced BMP signaling negatively regulates Drosophila midgut homeostasis. J Cell Biol 201, 945–961, doi:10.1083/jcb.201302049 (2013). [PubMed: 23733344]
17. Tracy Cai X et al. AWD regulates timed activation of BMP signaling in intestinal stem cells to maintain tissue homeostasis. Nat Commun 10, 2988, doi:10.1038/s41467-019-10926-2 (2019). [PubMed: 31278345]
18. Agaisse H, Petersen UM, Boutros M, Mathey-Prevot B & Perrimon N Signaling role of hemocytes in Drosophila JAK/STAT-dependent response to septic injury. Dev Cell 5, 441–450, doi:10.1016/s1534-5807(03)00244-2 (2003). [PubMed: 12967563]
19. Buchon N et al. Morphological and molecular characterization of adult midgut compartmentalization in Drosophila. Cell Rep 3, 1725–1738, doi:10.1016/j.celrep.2013.04.001 (2013). [PubMed: 23643535]
20. Tian A, Wang B & Jiang J Injury-stimulated and self-restrained BMP signaling dynamically regulates stem cell pool size during Drosophila midgut regeneration. Proc Natl Acad Sci U S A 114, E2699–E2708, doi:10.1073/pnas.1617790114 (2017). [PubMed: 28289209]
21. Dana H et al. High-performance calcium sensors for imaging activity in neuronal populations and microcompartments. Nat Methods 16, 649–657, doi:10.1038/s41592-019-0435-6 (2019). [PubMed: 31209382]
22. Li M, Sun S, Priest J, Bi X & Fan Y Characterization of TNF-induced cell death in Drosophila reveals caspase- and JNK-dependent necrosis and its role in tumor suppression. Cell Death Dis 10, 613, doi:10.1038/s41419-019-1862-0 (2019). [PubMed: 31409797]
23. Karpowicz P, Perez J & Perrimon N The Hippo tumor suppressor pathway regulates intestinal stem cell regeneration. Development 137, 4135–4145, doi:10.1242/dev.060483 (2010). [PubMed: 21098564]
24. Ren F et al. Hippo signaling regulates Drosophila intestine stem cell proliferation through multiple pathways. Proc Natl Acad Sci U S A 107, 21064–21069, doi:10.1073/pnas.1012759107 (2010). [PubMed: 21078993]
25. Dolan B, Ermund A, Martinez-Abad B, Johansson MEV & Hansson GC Clearance of small intestinal crypts involves goblet cell mucus secretion by intracellular granule rupture and enterocyte ion transport. Sci Signal 15, eabl5848, doi:10.1126/scisignal.abl5848 (2022). [PubMed: 36126118]
26. Masuyama K, Zhang Y, Rao Y & Wang JW Mapping neural circuits with activity-dependent nuclear import of a transcription factor. J Neurogenet 26, 89–102, doi:10.3109/01677063.2011.642910 (2012). [PubMed: 22236090]
27. Deng H, Gerencser AA & Jasper H Signal integration by Ca(2+) regulates intestinal stem-cell activity. Nature 528, 212–217, doi:10.1038/nature16170 (2015). [PubMed: 26633624]

Author Manuscript Author Manuscript Author Manuscript Author Manuscript

28. Xu C, Luo J, He L, Montell C & Perrimon N Oxidative stress induces stem cell proliferation via TRPA1/RyR-mediated Ca(2+) signaling in the Drosophila midgut. Elife 6, doi:10.7554/eLife.22441 (2017).
29. Amcheslavsky A et al. Enteroendocrine cells support intestinal stem-cell-mediated homeostasis in Drosophila. Cell Rep 9, 32–39, doi:10.1016/j.celrep.2014.08.052 (2014). [PubMed: 25263551]
30. Kumar A & Brockes JP Nerve dependence in tissue, organ, and appendage regeneration. Trends Neurosci 35, 691–699, doi:10.1016/j.tins.2012.08.003 (2012). [PubMed: 22989534]
31. Lai NY et al. Gut-Innervating Nociceptor Neurons Regulate Peyer's Patch Microfold Cells and SFB Levels to Mediate Salmonella Host Defense. Cell 180, 33–49 e22, doi:10.1016/j.cell.2019.11.014 (2020). [PubMed: 31813624]
32. Matheis F et al. Adrenergic Signaling in Muscularis Macrophages Limits Infection-Induced Neuronal Loss. Cell 180, 64–78 e16, doi:10.1016/j.cell.2019.12.002 (2020). [PubMed: 31923400]
33. Han H et al. Gut-neuron interaction via Hh signaling regulates intestinal progenitor cell differentiation in Drosophila. Cell Discov 1, 15006, doi:10.1038/celldisc.2015.6 (2015). [PubMed: 27462407]
34. Kenmoku H, Ishikawa H, Ote M, Kuraishi T & Kurata S A subset of neurons controls the permeability of the peritrophic matrix and midgut structure in Drosophila adults. J Exp Biol 219, 2331–2339, doi:10.1242/jeb.122960 (2016). [PubMed: 27229474]
35. Jenett A et al. A GAL4-driver line resource for Drosophila neurobiology. Cell Rep 2, 991–1001, doi:10.1016/j.celrep.2012.09.011 (2012). [PubMed: 23063364]
36. Kim AJ, Fenk LM, Lyu C & Maimon G Quantitative Predictions Orchestrate Visual Signaling in Drosophila. Cell 168, 280–294 e212, doi:10.1016/j.cell.2016.12.005 (2017). [PubMed: 28065412]
37. Tracey KJ Reflex control of immunity. Nat Rev Immunol 9, 418–428, doi:10.1038/nri2566 (2009). [PubMed: 19461672]
38. Babcock DT, Landry C & Galko MJ Cytokine signaling mediates UV-induced nociceptive sensitization in Drosophila larvae. Curr Biol 19, 799–806, doi:10.1016/j.cub.2009.03.062 (2009). [PubMed: 19375319]
39. Andersen DS et al. The Drosophila TNF receptor Grindelwald couples loss of cell polarity and neoplastic growth. Nature 522, 482–486, doi:10.1038/nature14298 (2015). [PubMed: 25874673]
40. Kanda H, Igaki T, Kanuka H, Yagi T & Miura M Wengen, a member of the Drosophila tumor necrosis factor receptor superfamily, is required for Eiger signaling. J Biol Chem 277, 28372–28375, doi:10.1074/jbc.C200324200 (2002). [PubMed: 12084706]
41. Doupe DP, Marshall OJ, Dayton H, Brand AH & Perrimon N Drosophila intestinal stem and progenitor cells are major sources and regulators of homeostatic niche signals. Proc Natl Acad Sci U S A 115, 12218–12223, doi:10.1073/pnas.1719169115 (2018). [PubMed: 30404917]
42. Harmansa S, Alborelli I, Bieli D, Caussinus E & Affolter M A nanobody-based toolset to investigate the role of protein localization and dispersal in Drosophila. Elife 6, doi:10.7554/eLife.22549 (2017).
43. Heir R & Stellwagen D TNF-Mediated Homeostatic Synaptic Plasticity: From in vitro to in vivo Models. Front Cell Neurosci 14, 565841, doi:10.3389/fncel.2020.565841 (2020). [PubMed: 33192311]
44. Petsakou A, Sapsis TP & Blau J Circadian Rhythms in Rho1 Activity Regulate Neuronal Plasticity and Network Hierarchy. Cell 162, 823–835, doi:10.1016/j.cell.2015.07.010 (2015). [PubMed: 26234154]
45. Ariyapala IS et al. Identification of Split-GAL4 Drivers and Enhancers That Allow Regional Cell Type Manipulations of the Drosophila melanogaster Intestine. Genetics 216, 891–903, doi:10.1534/genetics.120.303625 (2020). [PubMed: 32988987]
46. Petsakou A & Perrimon N Bioelectric regulation of intestinal stem cells. Trends Cell Biol, doi:10.1016/j.tcb.2022.10.003 (2022).
47. Harris MP Bioelectric signaling as a unique regulator of development and regeneration. Development 148, doi:10.1242/dev.180794 (2021).
48. Ho KYL, Khadilkar RJ, Carr RL & Tanentzapf G A gap-junction-mediated, calcium-signaling network controls blood progenitor fate decisions in hematopoiesis. Curr Biol 31, 4697–4712 e4696, doi:10.1016/j.cub.2021.08.027 (2021). [PubMed: 34480855]

Author Manuscript Author Manuscript Author Manuscript Author Manuscript

49. Dajas-Bailador FA, Mogg AJ & Wonnacott S Intracellular Ca2+ signals evoked by stimulation of nicotinic acetylcholine receptors in SH-SY5Y cells: contribution of voltage-operated Ca2+ channels and Ca2+ stores. J Neurochem 81, 606–614, doi:10.1046/j.1471-4159.2002.00846.x (2002). [PubMed: 12065669]

50. Kim AA et al. Independently paced Ca2+ oscillations in progenitor and differentiated cells in an ex vivo epithelial organ. J Cell Sci 135, doi:10.1242/jcs.260249 (2022).

Additional References:

51. Phillips MD & Thomas GH Brush border spectrin is required for early endosome recycling in Drosophila. J Cell Sci 119, 1361–1370, doi:10.1242/jcs.02839 (2006). [PubMed: 16537648]

52. Diao F et al. Plug-and-play genetic access to drosophila cell types using exchangeable exon cassettes. Cell Rep 10, 1410–1421, doi:10.1016/j.celrep.2015.01.059 (2015). [PubMed: 25732830]

53. Jenett A et al. A GAL4-driver line resource for Drosophila neurobiology. Cell Rep 2, 991–1001, doi:10.1016/j.celrep.2012.09.011 (2012). [PubMed: 23063364]

54. Ariyapala IS et al. Identification of Split-GAL4 Drivers and Enhancers That Allow Regional Cell Type Manipulations of the Drosophila melanogaster Intestine. Genetics 216, 891–903, doi:10.1534/genetics.120.303625 (2020). [PubMed: 32988987]

55. McGuire SE, Mao Z & Davis RL Spatiotemporal gene expression targeting with the TARGET and gene-switch systems in Drosophila. Sci STKE 2004, pl6, doi:10.1126/stke.2202004pl6 (2004). [PubMed: 14970377]

56. Brand AH & Perrimon N Targeted gene expression as a means of altering cell fates and generating dominant phenotypes. Development 118, 401–415 (1993). [PubMed: 8223268]

57. Dana H et al. High-performance calcium sensors for imaging activity in neuronal populations and microcompartments. Nat Methods 16, 649–657, doi:10.1038/s41592-019-0435-6 (2019). [PubMed: 31209382]

58. Lin S, Ewen-Campen B, Ni X, Housden BE & Perrimon N In Vivo Transcriptional Activation Using CRISPR/Cas9 in Drosophila. Genetics 201, 433–442, doi:10.1534/genetics.115.181065 (2015). [PubMed: 26245833]

59. Perkins LA et al. The Transgenic RNAi Project at Harvard Medical School: Resources and Validation. Genetics 201, 843–852, doi:10.1534/genetics.115.180208 (2015). [PubMed: 26320097]

60. Masuyama K, Zhang Y, Rao Y & Wang JW Mapping neural circuits with activity-dependent nuclear import of a transcription factor. J Neurogenet 26, 89–102, doi:10.3109/01677063.2011.642910 (2012). [PubMed: 22236090]

61. Chakraborty S et al. Mutant IP3 receptors attenuate store-operated Ca2+ entry by destabilizing STIM-Orai interactions in Drosophila neurons. J Cell Sci 129, 3903–3910, doi:10.1242/jcs.191585 (2016). [PubMed: 27591258]

62. Nern A, Pfeiffer BD & Rubin GM Optimized tools for multicolor stochastic labeling reveal diverse stereotyped cell arrangements in the fly visual system. Proc Natl Acad Sci U S A 112, E2967–2976, doi:10.1073/pnas.1506763112 (2015). [PubMed: 25964354]

63. Yagi R, Mayer F & Basler K Refined LexA transactivators and their use in combination with the Drosophila Gal4 system. Proc Natl Acad Sci U S A 107, 16166–16171, doi:10.1073/pnas.1005957107 (2010). [PubMed: 20805468]

64. Kitamoto T Conditional modification of behavior in Drosophila by targeted expression of a temperature-sensitive shibire allele in defined neurons. J Neurobiol 47, 81–92, doi:10.1002/neu.1018 (2001). [PubMed: 11291099]

65. Jovanic T et al. Competitive Disinhibition Mediates Behavioral Choice and Sequences in Drosophila. Cell 167, 858–870 e819, doi:10.1016/j.cell.2016.09.009 (2016). [PubMed: 27720450]

66. Potter CJ, Tasic B, Russler EV, Liang L & Luo L The Q system: a repressible binary system for transgene expression, lineage tracing, and mosaic analysis. Cell 141, 536–548, doi:10.1016/j.cell.2010.02.025 (2010). [PubMed: 20434990]

67. Hamada FN et al. An internal thermal sensor controlling temperature preference in Drosophila. Nature 454, 217–220, doi:10.1038/nature07001 (2008). [PubMed: 18548007]

Author Manuscript Author Manuscript Author Manuscript Author Manuscript

68. Nicolai LJ et al. Genetically encoded dendritic marker sheds light on neuronal connectivity in Drosophila. Proc Natl Acad Sci U S A 107, 20553–20558, doi:10.1073/pnas.1010198107 (2010). [PubMed: 21059961]
69. Harmansa S, Alborelli I, Bieli D, Caussinus E & Affolter M A nanobody-based toolset to investigate the role of protein localization and dispersal in Drosophila. Elife 6, doi:10.7554/eLife.22549 (2017).
70. Harrisingh MC, Wu Y, Lnenicka GA & Nitabach MN Intracellular Ca2+ regulates free-running circadian clock oscillation in vivo. J Neurosci 27, 12489–12499, doi:10.1523/JNEUROSCI.3680-07.2007 (2007). [PubMed: 18003827]
71. Nagarkar-Jaiswal S et al. A library of MiMICs allows tagging of genes and reversible, spatial and temporal knockdown of proteins in Drosophila. Elife 4, doi:10.7554/eLife.05338 (2015).
72. Ni JQ et al. A genome-scale shRNA resource for transgenic RNAi in Drosophila. Nat Methods 8, 405–407, doi:10.1038/nmeth.1592 (2011). [PubMed: 21460824]
73. Riabinina O et al. Improved and expanded Q-system reagents for genetic manipulations. Nat Methods 12, 219–222, 215 p following 222, doi:10.1038/nmeth.3250 (2015). [PubMed: 25581800]
74. Gratz SJ, Harrison MM, Wildonger J & O'Connor-Giles KM Precise Genome Editing of Drosophila with CRISPR RNA-Guided Cas9. Methods Mol Biol 1311, 335–348, doi:10.1007/978-1-4939-2687-9_22 (2015). [PubMed: 25981484]
75. Port F, Chen HM, Lee T & Bullock SL Optimized CRISPR/Cas tools for efficient germline and somatic genome engineering in Drosophila. Proc Natl Acad Sci U S A 111, E2967–2976, doi:10.1073/pnas.1405500111 (2014). [PubMed: 25002478]
76. Buchon N, Broderick NA, Poidevin M, Pradervand S & Lemaitre B Drosophila intestinal response to bacterial infection: activation of host defense and stem cell proliferation. Cell Host Microbe 5, 200–211, doi:10.1016/j.chom.2009.01.003 (2009). [PubMed: 19218090]
77. Ren F et al. Hippo signaling regulates Drosophila intestine stem cell proliferation through multiple pathways. Proc Natl Acad Sci U S A 107, 21064–21069, doi:10.1073/pnas.1012759107 (2010). [PubMed: 21078993]
78. Amcheslavsky A, Jiang J & Ip YT Tissue damage-induced intestinal stem cell division in Drosophila. Cell Stem Cell 4, 49–61, doi:10.1016/j.stem.2008.10.016 (2009). [PubMed: 19128792]
79. Kim K et al. Drosophila as a model for studying cystic fibrosis pathophysiology of the gastrointestinal system. Proc Natl Acad Sci U S A 117, 10357–10367, doi:10.1073/pnas.1913127117 (2020). [PubMed: 32345720]
80. Asano SM et al. Expansion Microscopy: Protocols for Imaging Proteins and RNA in Cells and Tissues. Curr Protoc Cell Biol 80, e56, doi:10.1002/cpcb.56 (2018). [PubMed: 30070431]
81. Li H et al. Fly Cell Atlas: A single-nucleus transcriptomic atlas of the adult fruit fly. Science 375, eabk2432, doi:10.1126/science.abk2432 (2022). [PubMed: 35239393]
82. Hu Y et al. FlyRNAi.org-the database of the Drosophila RNAi screening center and transgenic RNAi project: 2017 update. Nucleic Acids Res 45, D672–D678, doi:10.1093/nar/gkw977 (2017). [PubMed: 27924039]
83. Satyanarayan A, Moritz D, Wongsuphasawat K & Heer J Vega-Lite: A Grammar of Interactive Graphics. IEEE Trans Vis Comput Graph 23, 341–350, doi:10.1109/TVCG.2016.2599030 (2017). [PubMed: 27875150]
84. Hung RJ et al. A cell atlas of the adult Drosophila midgut. Proc Natl Acad Sci U S A 117, 1514–1523, doi:10.1073/pnas.1916820117 (2020). [PubMed: 31915294]
85. Chen J, Xu N, Huang H, Cai T & Xi R A feedback amplification loop between stem cells and their progeny promotes tissue regeneration and tumorigenesis. Elife 5, doi:10.7554/eLife.14330 (2016).
86. https://app.biorender.com

Author Manuscript Author Manuscript Author Manuscript Author Manuscript

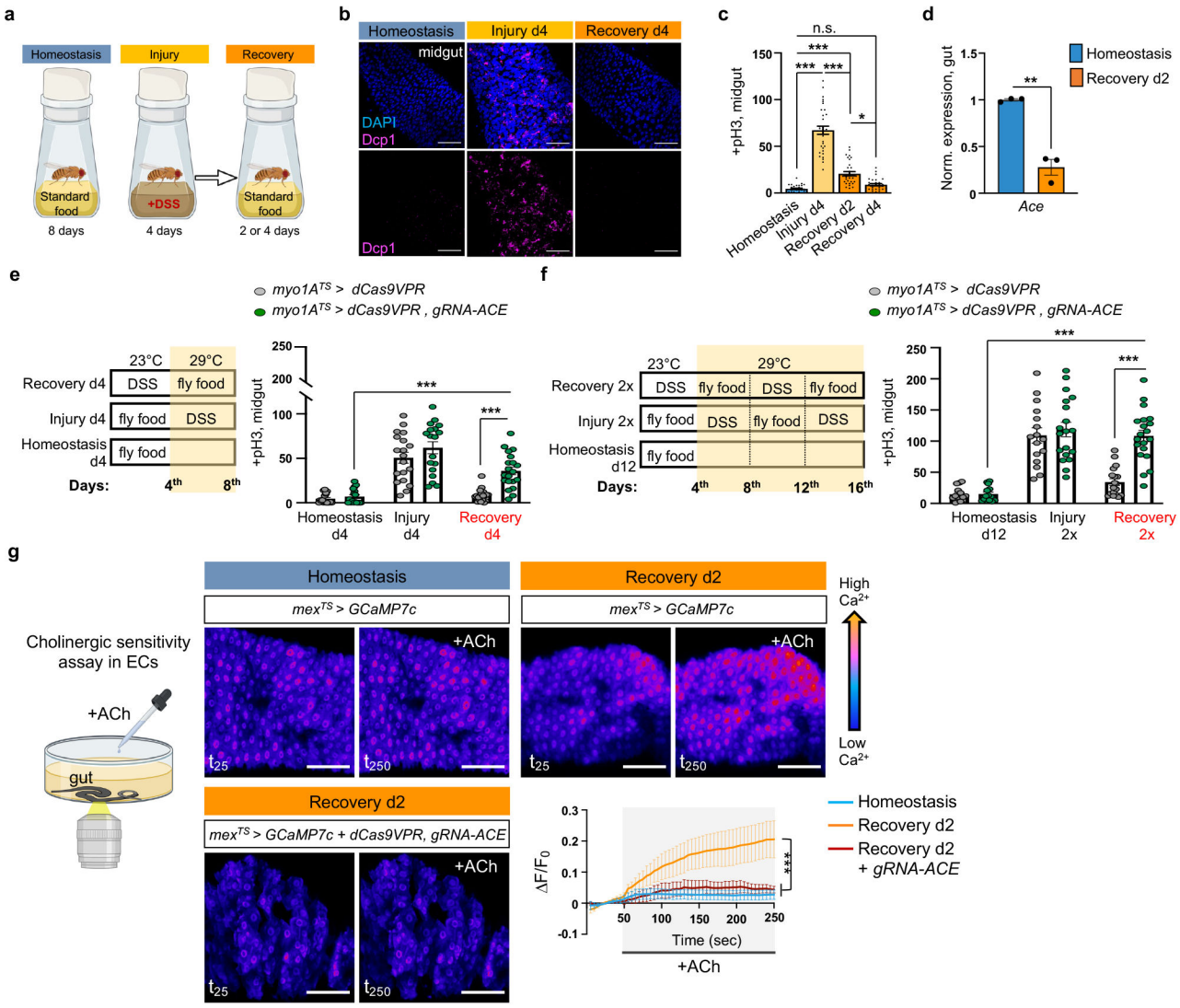

Fig.1 |. ACh sensitivity is required for recovery.

a, Experimental design illustration. Midgut of *OreR* flies with cell death marker anti-Dcp1 (*Drosophila* caspase 1, magenta) and DAPI (nuclei, blue). Conditions like 1a at 29°C. Images are representative of two independent experiments with similar results. scale bar: 50μm. **c,** Mitotic division counts of proliferating ISCs in the midgut of *Ore R* flies with anti-PhoshoHistone-3 (pH3) staining (conditions like Fig.1b). n=29 xDunn's Kruskal-Wallis test : p=0.02 (Rec. d2 vs Rec. d4). Black dots indicate counts per gut. **d,** Expression levels of *Ace* in *Ore R* guts. Normalized to Homeostasis. n=3 biologically independent samples per condition (two-tailed t-test, p=0.0011). **e-f,** Experimental design and graphs of pH3+ counts from control (*myo1A^{TS}>dCas9VPR*) and flies with *Ace* conditionally overexpressed in ECs (*myo1A^{TS}>dCas9VPR, gRNA-Ace*). Conditional perturbations with temperature-sensitive Gal4 inhibitor, *Tubulin-Gal80^{TS}*(^{TS}), allow Gal4 expression only >27°C. control: n=18(Homeostasis),19(Injury), 20(Recovery), 15(Homeostasis d12), 16(Injury 2x), 18(Recovery 2x) guts ; *gRNA-Ace*: n=17(Homeostasis), 18(Injury), 20(Recovery),14(Homeostasis d12),19(Injury 2x),

Author Manuscript Author Manuscript Author Manuscript Author Manuscript

20(Recovery 2x) guts, from 3 independent experiments. Sidak's and Tukey's two-way Anova. **g,** Assay illustration and color-coded sequential frames of midgut before (t_{25}) and after (t_{250}) ACh administration of flies conditionally expressing the Ca^{2+} reporter GCAMP7c with the EC-driver *mex1*-Gal4 (*mex^{TS} >GCaMP7c*) and flies overexpressing *Ace* (*mex^{TS} >GCaMP7c+dCas9VPR,gRNA-Ace*, Videos S1-S3). Recovery: 2 days in standard food (29°C) after 4 days of DSS-feeding (23°C). Homeostasis: conditions like Recovery without DSS-feeding. Accompanying graph: average relative fluorescence intensity ($\Delta F/F_0$) per frame (5 sec/frame) and genotype. n=7 (Homeostasis), n=7 (Recovery d2), n=5 (Recovery d2, *mex^{TS}> gRNA-Ace*) guts, from 3 independent experiments. Tukey's two-way Anova. Individual $\Delta F/F_0$ shown on Ext. Data Fig.2i. scale bar: 50μm *: 0.05>p>0.01, **: 0.01<p<0.001, ***: p<0.001, ns: non-significant. Data are presented as mean values ± SEM. Illustrations with Biorender.com

Author Manuscript Author Manuscript Author Manuscript Author Manuscript

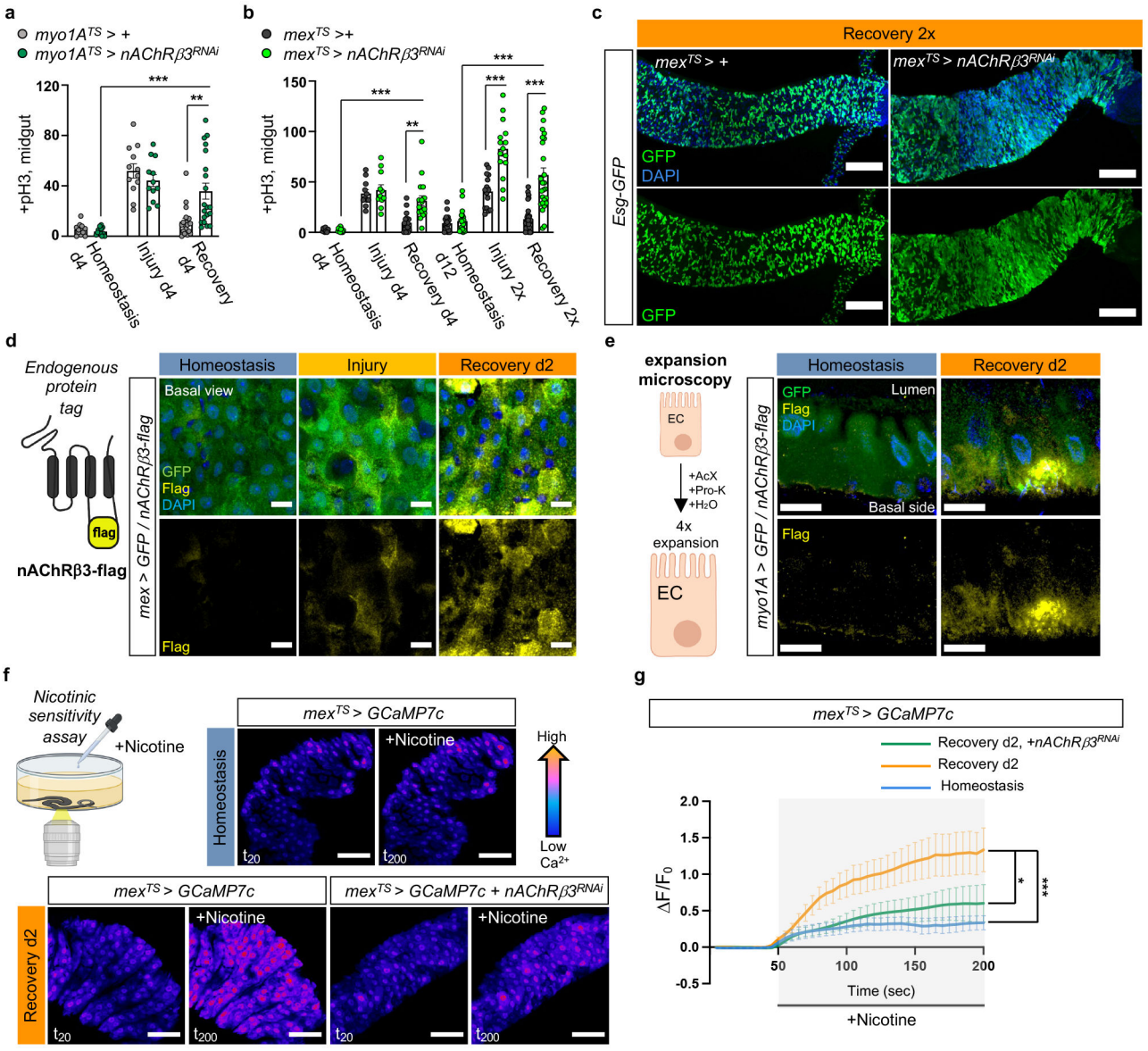

Fig.2 |. nAChRβ3 is required in ECs for recovery.

a, pH3+ counts from midgut of control (*myo1A^{TS} > +*) and flies with *nAChRβ3* conditionally reduced in ECs (*myo1A^{TS}> nAChRβ3^{RNAi}*). control: n=13 (Homeostasis), n=12(Injury), n=18(Recovery) guts, *myo1A^{TS}>nAChRβ3^{RNAi}*: n=13 (Homeostasis), n=12(Injury), n=20 (Recovery) guts, from 2 independent experiments. Sidak's and Tukey's two-way Anova. Like Fig. 1e. **b,** pH3+ counts from midgut of control (*mex^{TS} > +*) and flies with *nAChRβ3* conditionally reduced in ECs (*mex^{TS}>nAChRβ3^{RNAi}*). control: n=12 (Homeostasis), n=11(Injury), n=18(Recovery), n=20(Homeostasis d12), n=15(Injury 2x), n=29 (Recovery 2x); *mex^{TS}>nAChRβ3^{RNAi}*: n=12 (Homeostasis), n=11 (Injury), n=17 (Recovery), n=20 (Homeostasis d12), n=15 (Injury 2x), n=26(Recovery 2x), from 3 independent experiments. Sidak's and Tukey's two-way Anova. Like Fig. 1e-f. **c,** Confocal gut images of *mex^{TS}>+* and *mex^{TS}>nAChRβ3^{RNAi}* flies co-expressing the PC marker esg-GFP (green, anti-GFP, like Fig. 2b). scale bar: 100μm. Images are representative of 2

Author Manuscript Author Manuscript Author Manuscript Author Manuscript

independent experiments with similar results. **d,** Illustration of nAChRβ3-flag and confocal images of midgut expressing nAChRβ3-flag and GFP-expressing ECs (*mex >GFP*). anti-Flag: nAChRβ3-flag (yellow), anti-GFP: ECs (green). scale bar: 10μm. Images are representative of 3 independent experiments with similar results. Like Fig. 1e. **e,** Illustration followed by images of expanded midguts from flies expressing nAChRβ3-flag (yellow) and GFP-expressing ECs (*myo1A >GFP,* green). scale bar: 50μm. Images are representative of 2 independent experiments with similar results. **f-g,** Illustration and color-coded sequential frames of midgut before (t_{20}) and after (t_{200}) nicotine administration of $mex^{TS} > GCaMP7c$ and $mex^{TS >} GCaMP7c{+}nAChR\beta3^{RNAi}$ flies (Videos S4-S6). Bottom graph: average relative fluorescence intensity ($\Delta F/F_0$) per frame (5 sec/frame) per condition and genotype. n=7(Homeostasis),n=7(Recovery d2),n=5 (Recovery d2, $mex^{TS}>Ace$) guts from 2 independent experiments. Tukey's two-way Anova (Rec d2 vs Rec d2+$nAChR\beta3^{RNAi}$, p=0.0116). Like Fig 1g. scale bar: 50μm. Individual $\Delta F/F_0$ on Ext. Data Fig.3k. DAPI: nuclei. *: 0.05>p>0.01, **: 0.01<p<0.001, ***: p<0.001. Mean ± SEM. Illustrations with Biorender.com

Author Manuscript Author Manuscript Author Manuscript Author Manuscript

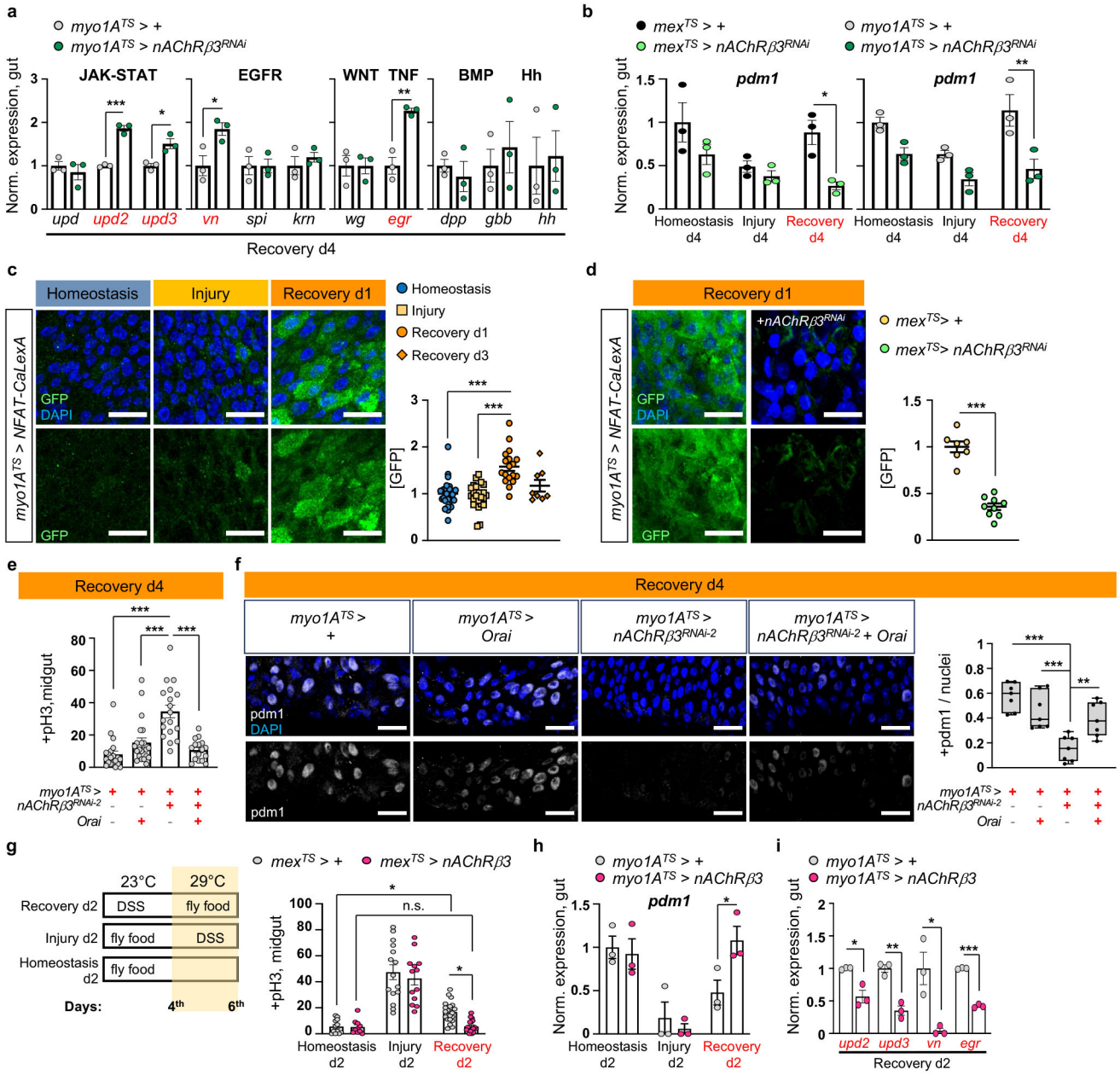

Fig.3 |. nAChRβ3-mediated Ca^{2+} promotes recovery.

a, Cytokine expression levels when reducing *nAChRβ3* in ECs (*myo1A^{TS}>nAChRβ3^{RNAi}*). Like Fig. 1e. *upd*(*unpaired*), *vn*(*vein*), *spi*(*spitz*), *krn*(*keren*), *wg*(*wingless*), *dpp*(*decapentaplegic*), *gbb*(*glass bottom boat*), *hh*(*hedgehog*). n=3 biologically independent samples per genotype. Sidak's two-way Anova; p=0.0196(*vn*), p=0.0022 (*egr*).

b, *Pdm1* levels when reducing *nAChRβ3* in ECs (*mex^{TS}>nAChRβ3^{RNAi}* and *myo1A^{TS}>nAChRβ^{RNAi}*). Like Fig. 1e. n=3 biologically independent samples per genotype and condition. Sidak's two-way Anova; p=0.0014 (Rec.d4, *myo1A^{TS}>+* vs *myo1A^{TS}>nAChRβ3^{RNAi}*), p=0.0142 (Rec.d4, *mex^{TS}>+* vs *mex^{TS}>nAChRβ3^{RNAi}*).

c, Posterior midgut with Ca^{2+} reporter in ECs (*myo1A^{TS}>NFAT-CaLexA*). Reporter

Author Manuscript Author Manuscript Author Manuscript Author Manuscript

expression: 2days (29°C) per condition. GFP: green(Ca^{2+}). Graph: GFP per image and condition. n=25(Homeostasis), n=24(Injury),n=18(Rec.d1), n=8(Rec.d3) guts from 3 independent experiments (Dunn's Kruskal-Wallis test). **d,** Posterior midgut with NFAT-CaLexA in control (*mex^{TS}>NFAT-CaLexA)* and when reducing *nAChRβ3* in ECs (*mex^{TS}>NFAT-CaLexA+$nAChRβ3^{RNAi}$*). Conditions: 4days DSS-food (23°C) and standard food for 24hrs (29°C). n=7(control), n=9(*$nAChRβ3^{RNAi}$*) guts from 2 independent experiments (two-tailed t-test). **e,** pH3+ counts from Orai (Ca^{2+} channel) overexpression (*$myo1A^{TS}$>Orai*), *nAChRβ3* reduction (*$myo1A^{TS}$>$nAChRβ3^{RNAi-2}$*) and combined (*$myo1A^{TS}$>$nAChRβ3^{RNAi}$+Orai*) in ECs. Like Fig 1e. n=20(control), n=22(*Orai*), n=18(*$nAChRβ3^{RNAi2}$*), n=16(*$nAChRβ3^{RNAi}$ +Orai*) guts, from 3 independent experiments (Dunn's Kruskal-Wallis test). **f,** Posterior midgut stained with anti-pdm1(grey), like Fig. 3e. Boxplot: pdm1+ versus all nuclei per image (median, quartiles, whiskers: minimum maximum values). N=7 guts per genotype (Tukey's one-way Anova, Orai vs *$nAChRβ3^{RNAi}$ + Orai*: p=0.0092), from 2 independent experiments. **g,** Experimental design and pH3+ counts when *nAChRβ3* is overexpressed in ECs (*mex^{TS}>nAChRβ3*). control: n=12(Hom.), n=15(Injury), n=21(Rec.d2) guts, *mex^{TS}>nAChRβ3*: n=8(Hom.), n=13(Injury), n=18(Rec.d2) guts from 2 independent experiments. Two-way Anova: p=0.023 (Rec. d2: control vs *mex^{TS}>nAChRβ3*), p=0.0396 (control: Hom. vs Rec.d2). **h-i,** *Pdm1* and cytokine levels from *$myo1A^{TS}$>nAChRβ3* flies. Like Fig. 3g. n=3 biologically independent samples per genotype. Sidak's two-way Anova (*pdm1*/Rec.d2: p=0.0415, *upd2*: p=0.0326, *upd3*: p=0.0014, *egr*: p=0.0037). DAPI: nuclei. scale bars: 20μm. *: 0.05>p>0.01, **: 0.01<p<0.001, ***: p<0.001. n.s.: non-significant. Mean ± SEM.

Author Manuscript Author Manuscript Author Manuscript Author Manuscript

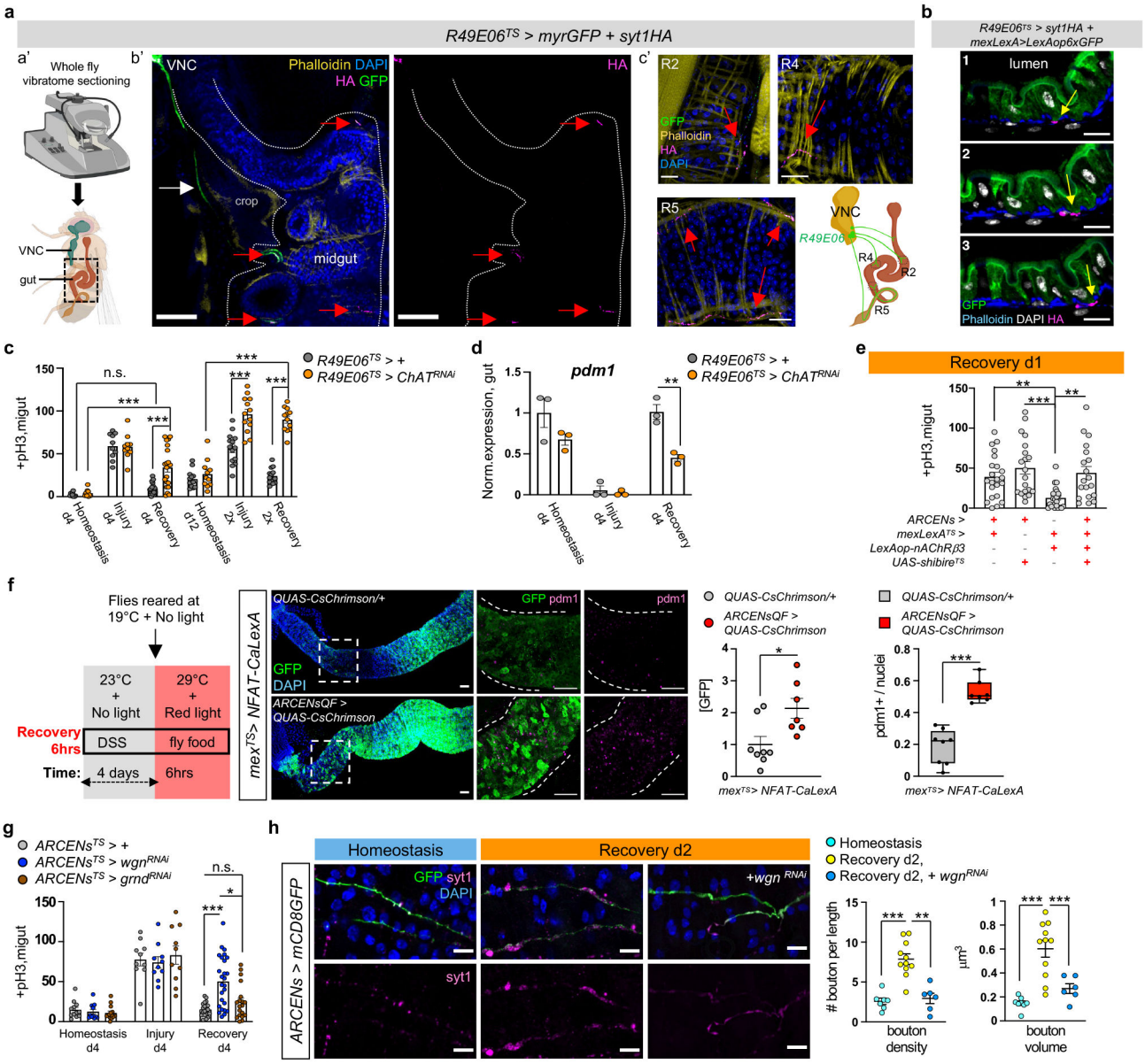

Fig.4 |. ARCEN-EC interactions promote recovery.

a, Vibratome-sectioning of *R49E06^{TS}>myrGFP+syt1HA* flies (Rec.d2). a'-b': sectioned thorax/abdomen (square). white dots: midgut. White arrow: R49E06-projection. c': innervated R2, R4, R5. anti-GFP: R49E06-innervations(green), anti-HA: presynaptic syt1HA(magenta). Red arrow: R49E06-enteric innervations. Images b'-c' are representative of 2 independent experiments with similar results. scale bar: 100μm(b'), 20μm(c'). **b,** Sequential R4 images (Video S7) from R49E06^{TS}*>syt1HA+mexLexA>6xLexAopGFP* flies (Rec.d2). Arrows: anti-HA(magenta), anti-GFP: ECs(green). scale bar: 10μm. Images are representative of 2 independent experiments with similar results. **c,** +pH3 counts when *ChAT* (*Choline Acetyltransferase*) is reduced in R49E06-neurons (*R49E06^{TS}>ChAT^{RNAi}*). Control: n=10(Hom.), n=10(Injury), n=16(Rec.d4), n=13(Hom.d12), n=14 (Injury 2x),n=13(Rec.2x) guts; *R49E06^{TS}>ChAT^{RNAi}*: n=

Author Manuscript Author Manuscript Author Manuscript Author Manuscript

10(Hom.), n=10(Injury), n=20(Rec.d4),n=11(Hom.d12),n=13(Injury 2x),n=12(Rec.2x) guts, from 2 independent experiments (Sidak's two-way Anova). Like Fig.1e-f. **d,** *Pdm1* expression levels. n=3 biologically independent samples. Sidak's two-way Anova(p=0.0027). **e,** +pH3 counts when overexpressing *nAcRβ3* in ECs (*mexLexA^{TS}>lexAop-nAcRβ3*) and thermo-silencing (>27°C) *R49E06*/ARCENs with *shibire^{TS}* (*ARCENs>shibire^{TS}*). Conditions: 4days DSS-food (23°C), 24hrs standard food (29°C). n=22(control), n=20(*ARCENs>shibire^{TS}*), n=24(*mexLexA^{TS}>lexAop-nAcRβ3*), n=19(*ARCENs>shibire^{TS}+mexLexA^{TS}>lexAop-nAcRβ3*) guts from 3 independent experiments. Dunn's Kruskal-Wallis test: p=0.0029(control vs *shibire^{TS}*), p=0.0024(*shibire^{TS}+lexAop-nAcRβ3* vs *shibire^{TS}*). **f,** Thermo- and optogenetic induction with NFAT-CalexA expressed in ECs (*mex^{TS}>NFAT-CaLexA/QUAS-CsChrimson*) after depolarizing ARCENs with CsChrimson (*mex^{TS}>NFAT-CaLexA/ARCENsQF>QUAS-CsChrimson*). anti-GFP: Ca^{2+}(green), anti-pdm1: ECs(magenta). Chart: GFP fold change, Boxplot: pdm1+ ratio (median, quartiles, whiskers: minimum maximum values). n=8(control), n=7(CsChrimson) guts from two independent experiments, two-tailed Mann-Whitney test (p=0.0205/GFP). scale bar: 50μm. **g,** pH3+ counts after reducing TNF receptors in ARCENs (*wgn*/*wengen*, *ARCENs^{TS}>wgn^{RNAi}* ; *grnd*/*grindelwald*, *ARCENs^{TS}>grnd^{RNAi}*). control: n=12(Hom.), n=10(Injury), n=21(Rec.); *wgn^{RNAi}*: n=12(Hom.), n=10(Injury), n=25(Rec.); *grnd^{RNAi}*: n=14(Hom.), n=10(Injury), n=19(Rec.) guts from 2 independent experiments. Dunn's Kruskal-Wallis test: p=0.0185(*wgn^{RNAi}* vs *grnd^{RNAi}*; Rec). **h,** R5 of ARCENs>*mCD8GFP* and ARCENs>*mCD8GFP+wgn^{RNAi}* guts. anti-GFP: ARCENs-innervations(green), anti-Syt1: boutons(magenta). n=8(Hom.), n=11(Rec.), n=6(*wgn^{RNAi}*) guts, from 2 independent experiments. Tukey's one-way Anova (p=0.0019, Rec. vs *wgn^{RNAi}*; boutons). scale bar: 10μm. Phalloidin: muscle. DAPI: nuclei. *: 0.05>p>0.01, **:0.01<p<0.001, ***:p<0.001. n.s.: non-significant. Mean ± SEM. Illustrations with Biorender.com

Author Manuscript Author Manuscript Author Manuscript Author Manuscript

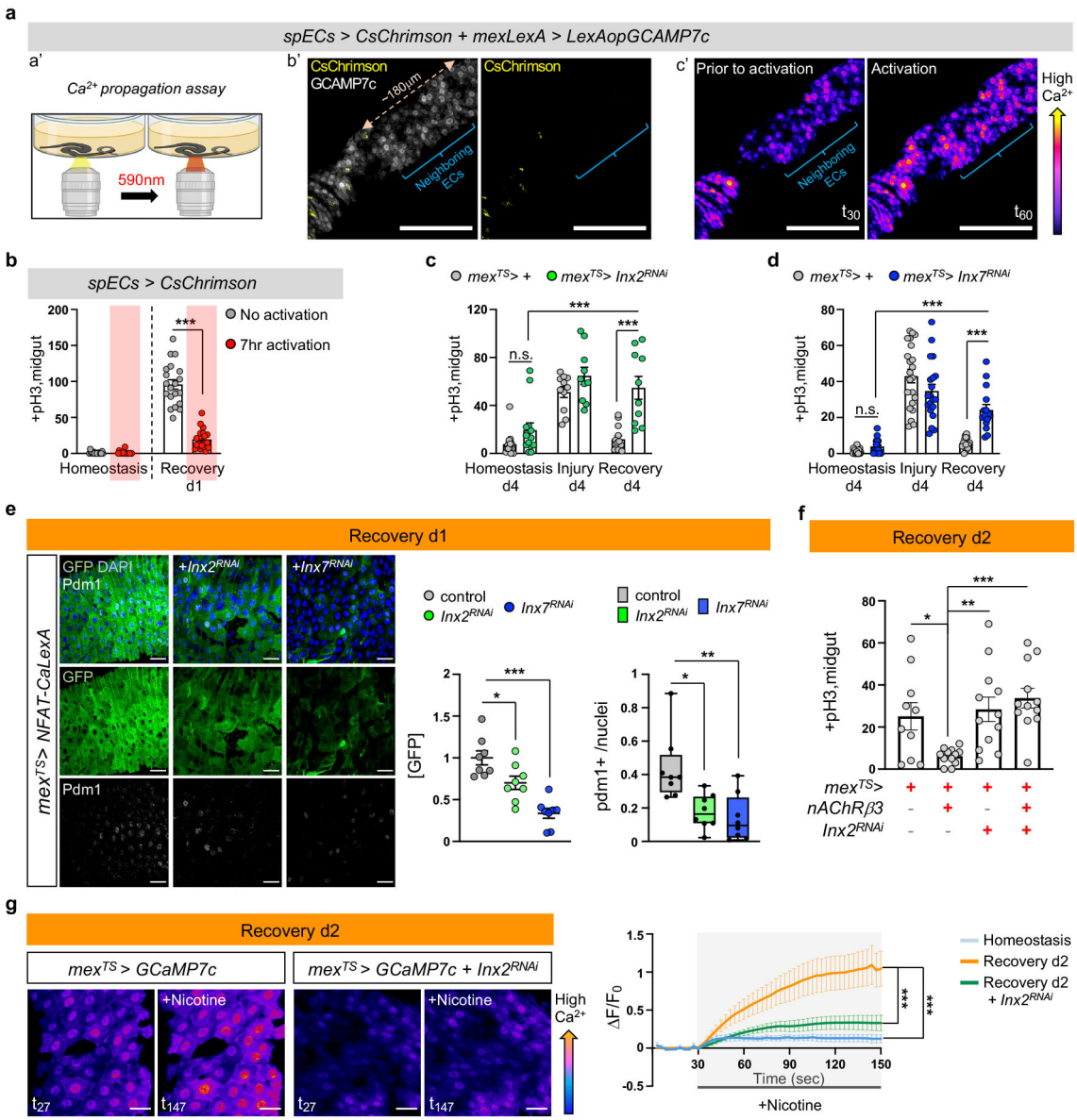

Fig.5 | Ca^{2+} spreads via Inx2/Inx7 gap junctions.

a, a': Experimental Illustration. b': Posterior midgut with *CsChrimson* in few ECs (spECs, *spEC>CsChrimson*, yellow) while all ECs express *GCAMP7c* (*mexLexA>LexAopGCAMP7c,* grey). Neighboring ECs: no CsChrimson expression. c': Color-coded sequential frames prior (t_{30}) and during (t_{60}) CsChrimson-activation (Video S8). Images are representative of 3 independent experiments with similar results. Quantifications: Ext. Data Fig.8b. scale bar: 100µm. **b,** pH3+ counts of *spEC>CsChrimson* during 7hr opto-activation. No activation: n=17(Hom.), 20(Rec.) ; Activation: n=16(Hom.), n=21(Rec.) guts from 3 independent experiments (two-tailed Mann-Whitney). Conditions: see Methods. **c-d,** pH3+ counts when reducing *Inx2* (*mex^{TS}>$Inx2^{RNAi}$*) and *Inx7* (*mex^{TS}>$Inx7^{RNAi}$*) in ECs. Conditions: Fig. 1e. control: n=13(Hom./c), n=23(Hom./d), n=11(Injury/c), n=22(Injury/d), n=13(Rec./c), n=16(Rec./d); *$Inx2^{RNAi}$*: n=13(Hom.), n=10(Injury), n=10(Rec); *$Inx7^{RNAi}$*: n=17(Hom.), n=20(Injury),

Author Manuscript Author Manuscript Author Manuscript Author Manuscript

n=15(Rec.) guts from 2 independent experiments (two-way Anova). **e,** Posterior midgut expressing NFAT-CaLexA in ECs while reducing *Inx2* or *Inx7* (*mex^{TS}>NFAT-CaLexA+Inx2^{RNAi}*, *mex^{TS}>NFAT-CaLexA+Inx7^{RNAi}*). anti-GFP: Ca^{2+}(green), anti-pdm1: ECs(grey). DAPI: nuclei. Scalebar 20μm. Conditions: 4days DSS-food (23°C), 24hrs standard food (29°C). Chart: GFP fold change, Boxplot: pdm1+ ratio (median, quartiles, whiskers: minimum maximum values). n=8 guts per genotype from 2 independent experiments. Tukey's one-way Anova (p=0.0272; control vs *Inx2^{RNAi}*; GFP). Dunn's Kruskal-Wallis test (p=0.024 control vs *Inx2^{RNAi}*;pdm1+), **f,** pH3+ counts when overexpressing *nAcRβ3* (*mex^{TS}>nAcRβ3),* reducing *Inx2* in ECs (*mex^{TS}>Inx2^{RNAi}*) and combined (*mex^{TS}>nAcRβ3+Inx2^{RNAi}*). Conditions: 4days DSS-food (23°C), 48hrs standard food (29°C). n=10(*mex^{TS}>+*), n=12(*mex^{TS}>nAcRβ3*, *mex^{TS}>Inx2^{RNAi}*, *mex^{TS}>nAcRβ3+Inx2^{RNAi}*) guts from 2 independent experiments. Tukey's one-way Anova (p=0.0476 control vs *nAcRβ3,* p=0.0096 *nAcRβ3* vs *Inx2^{RNAi}*). **g,** Color-coded sequential frames while reducing *Inx2* in ECs (*mex^{TS} >GCaMP7c+Inx2^{RNAi}*) before (t_{27}) and after (t_{147}) nicotine (Videos S9-S10). Graph: average fluorescence intensity ($\Delta F/F_0$) per frame (~3sec/fr) and genotype. Individual $\Delta F/F_0$: Ext. Data Fig.8k. n= 6(Hom.), n=9(Rec.),n=8(*Inx2^{RNAi}*) guts from 2 independent experiments (Tukey's two-way Anova). scale bar: 20μm. Conditions: Fig. 2f. n.s.:non-significant, *: 0.05>p>0.01, **: 0.01<p<0.001, ***: p<0.001. Mean ± SEM. Illustrations with Biorender.com